

1 Multiday production of condensing organic aerosol mass in
2 urban and forest outflow

3

4 Julia Lee-Taylor¹, Alma Hodzic¹, Sasha Madronich¹, Bernard Aumont², Marie
5 Camredon², Richard Valorso²

6

7 ¹National Center for Atmospheric Research, Boulder, CO 80307, USA

8 ²Laboratoire Interuniversitaire des Systèmes Atmosphériques, UMR 7583, CNRS, Université Paris Est
9 Créteil et Université Paris Diderot, 94010, Créteil, France

10

11 Abstract

12 Secondary organic aerosol (SOA) production in air masses containing either anthropogenic or
13 biogenic (terpene-dominated) emissions is investigated using the explicit gas-phase chemical
14 mechanism generator GECKO-A. Simulations show several-fold increases in SOA mass continuing for
15 multiple days in the urban outflow, even as the initial air parcel is diluted into the regional
16 atmosphere. The SOA mass increase in the forest outflow is more modest (~ 50%) and of shorter
17 duration (1-2 days). The multiday production in the urban outflow stems from continuing oxidation
18 of gas-phase precursors which persist in equilibrium with the particle phase, and can be attributed
19 to multigenerational reaction products of both aromatics and alkanes, especially those with
20 relatively low carbon numbers (C4-15). In particular we find large contributions from substituted
21 maleic anhydrides and multi-substituted peroxide-bicyclic alkenes. The results show that the
22 predicted production is a robust feature of our model even under changing atmospheric conditions
23 and different vapor pressure schemes, and contradict the notion that SOA undergoes little mass
24 production beyond a short initial formation period. The results imply that anthropogenic aerosol
25 precursors could influence the chemical and radiative characteristics of the atmosphere over an
26 extremely wide region, and that SOA measurements near precursor sources may routinely
27 underestimate this influence.

28

29 **1 Introduction**

30 The contribution of anthropogenic aerosol is one of the greatest current uncertainties in the
31 assessment of climate forcing (e.g. Forster et al., 2007). Organic aerosol (OA) comprises a significant

1 (20-90%) fraction of anthropogenic aerosol (Kanakidou et al., 2005; Jimenez et al., 2009; Zhang et al.,
2 2007). OA consists, to a first approximation, of both primary organic aerosol (POA) directly emitted
3 as particles in evaporative equilibrium with the gas phase (Robinson et al., 2007), and the much
4 more abundant secondary organic aerosol (SOA) produced by condensation of oxidation products of
5 gas-phase VOC (volatile organic compound) precursors (e.g. Kanakidou et al., 2005; Jimenez et al.,
6 2009). Climate uncertainties stem from both the difficulty in characterizing the radiatively-important
7 interactions of OA given its globally non-uniform composition (McFiggans et al., 2006), and from the
8 difficulty in simulating its abundance and distribution (e.g. Goldstein and Galbally, 2007; Hallquist et
9 al., 2009).

10 Radiative impacts of atmospheric aerosols fall into two main categories, aerosol-radiation
11 interactions and aerosol-cloud interactions (e.g. Forster et al., 2007; Boucher et al., 2013). Aerosol-
12 radiation interactions encompass absorption and scattering of solar radiation by aerosol particles
13 (also known as the direct effect) and cloud evaporation due to the consequent atmospheric heating
14 (semi-direct effects). Widely different estimates of direct radiative forcing are produced by differing
15 estimates of global SOA mass burdens (Tsigaridis et al., 2014, after Myhre et al., 2013, and Spracklen
16 et al., 2011). Aerosol-cloud interactions (indirect effects) encompass a range of cloud properties
17 influenced by aerosols acting as cloud condensation nuclei (CCN). The relationship between CCN
18 number and radiative forcing is itself complex and model parameterizations vary substantially
19 (Boucher et al., 2013). Recent studies attribute about one-third of the total uncertainty in modeled
20 CCN concentrations to uncertainties in SOA production (Carslaw et al., 2013), and find that CCN
21 concentrations are sensitive to the relative proportions of POA and SOA (Trivitayanurak and Adams,
22 2014) and to oxidative ageing (Yu, 2011). These results show the importance of representing sources
23 and life cycle processes that affect the mass and other climate-relevant properties of SOA in as
24 realistic and physically-based a way as possible.

25 Laboratory-based descriptions of SOA formation and yields have become increasingly complex. Early
26 calculations used precursor-specific 2-product formulations (Odum et al., 1996) which describe smog
27 chamber OA mass yields reasonably well but produce significant underestimates of atmospheric OA
28 in both near-source regions and in the free troposphere (e.g. Volkamer et al., 2006; Heald et al.,
29 2011). The VBS (volatility basis set) framework (Donahue et al., 2006) uses empirical volatility
30 distributions to describe multi-species particle-gas mixtures and their chemical transformations
31 (ageing) over laboratory timescales (Grieshop et al., 2009; Robinson et al., 2007). This concept
32 broadly designates SVOCs (semi-volatile organic compounds), species with significant fractions in
33 both gas and particle phases, and IVOCs (intermediate-volatility organic compounds), gas phase
34 species whose products are likely to condense as SOA (Donahue et al., 2009). VBS formulations have

1 improved SOA estimates in numerous model studies e.g. (Tsimpidi et al., 2010; Lane et al., 2008;
2 Dzepina et al., 2011; Zhang et al., 2013). However the ageing parameterizations are often tuned to
3 match observed OA mass distributions e.g. (Jo et al., 2013), and as such are not generalizable. In
4 efforts to incorporate more chemical complexity and realism to representations of bulk organic
5 aerosol properties and evolution, various two-dimensional schemes have been developed e.g. (Kroll
6 et al., 2011; Donahue et al., 2012; Pankow and Barsanti, 2009; Barsanti et al., 2013) and
7 implemented in regional e.g. (Murphy et al., 2012) and global e.g. (Mahmud and Barsanti, 2013)
8 models. Other model studies have increased the number of OA precursor types represented e.g.
9 (Pye and Pouliot, 2012), or added SOA production in cloud drops e.g. (Lin et al., 2012). These
10 modeling advances have reduced, but not eliminated the gaps between predictions and ambient
11 measurements of SOA.

12 The difficulty in reproducing observed aerosol mass distributions is partly attributable to the
13 mismatch between the timescales accessible to laboratory studies, and the atmospheric lifetimes of
14 OA and its precursor gases. OA lifetimes are generally considered to be of the order of about a week
15 (Boucher et al, 2013) or more (Kristiansen et al., 2012), during which the airborne particles are
16 continually subject to ageing processes. The dynamic nature of gas-particle condensation equilibria
17 (Pankow, 1994b) allows for evaporation-oxidation-re-condensation cycling of OA constituents,
18 altering the chemical composition including the relative proportions of POA and SOA. In addition,
19 the continual chemical evolution of the associated gas phase implies product volatility changes on
20 timescales of several days (Kroll and Seinfeld, 2008), opening the possibility of multi-day SOA
21 formation. By contrast, practical considerations typically limit aerosol chamber studies to a few
22 hours, although a few recent studies have achieved effective photochemical timescales of up to 3
23 days e.g. (Yee et al., 2012; Craven et al., 2012). Field observation of long-term aerosol evolution is
24 also challenging owing to dilution and mixing of outflow plumes with regional air. SOA production in
25 various plumes has been assessed by normalizing OA to ΔCO , the difference between plume and
26 background CO values, e.g. (Kleinman et al. , 2008; DeCarlo et al., 2010) and references therein. Such
27 observations generally extend to photochemical ages of \sim 1 day (DeCarlo et al., 2010). Ship-borne OA
28 and CO observations in urban plumes with transport-based ages of up to about 4 days have clearly
29 shown SOA production for \sim 2 days, with large data scatter thereafter (de Gouw et al., 2008).

30 Another problem of scale is inherent in the sheer number of potential chemical reactions and
31 products leading to SOA formation (e.g. Goldstein and Galbally, 2007). Indeed, recent advances in
32 high resolution mass spectrometry analytical techniques have enabled characterization of many
33 hundreds of individual OA constituents (e.g. Nizkorodov et al., 2011 and references therein; Chan et
34 al., 2013; O'Brien et al, 2013; Kourtchev et al, 2014)). Explicit modeling of hydrocarbon chemistry

1 involves potentially millions of intermediate species (Aumont et al., 2005). This can be simplified to
2 only a few hundred species when considering ozone production (Szopa et al., 2005), but is far more
3 complicated for SOA production (Camredon et al., 2007; Valorso et al., 2011; Aumont et al., 2013;
4 Aumont et al., 2012) which is not dominated by any one species but rather results from
5 condensation of many oxygenated intermediates and their in-particle transformations.

6 The atmospheric chemical processes leading to the formation of condensable vapors and ultimately
7 to SOA may be simulated explicitly, using structure-activity relationships based on laboratory
8 measurements of individual and fundamental chemical kinetic rates and pathways. We have
9 previously used the explicit model GECKO-A to simulate SOA formation in the urban outflow plume
10 from Mexico City (Lee-Taylor et al., 2011, hereinafter L-T11). That study showed OA mass production
11 continuing for several days and yielding several times the regionally-integrated SOA mass that would
12 be implied from concentrations near the source. In this work, we use sensitivity studies and case
13 studies with both urban and biogenic emissions assemblages to examine whether the modeled OA
14 mass production is a robust feature of our model, and to elucidate the chemical identities of the
15 species responsible.

16

17 **2 Approach**

18 **2.1 The GECKO-A Model**

19 GECKO-A (Generator of Explicit Chemistry and Kinetics of Organics in the Atmosphere) is an
20 automatic generator for atmospheric gas-phase chemical mechanisms. It is described in detail by
21 (Aumont et al., 2005), with updates by (Camredon et al., 2007; Aumont et al., 2008; Valorso et al.,
22 2011), and as described here. The atmospheric oxidation of aliphatic compounds is treated explicitly
23 based directly on laboratory measurements if available, or on structure-activity relationships (SARs)
24 where data are not available. The chemical mechanism for the oxidation of aromatic compounds is
25 taken from the Master Chemical Mechanism, MCM v3.1 (Jenkin et al., 2003; Bloss et al., 2005a) up
26 to the loss of the aromatic structures, and computed from GECKO-A for subsequent chemistry.
27 Photochemistry is driven by a j-value lookup table, calculated using the TUV (Tropospheric
28 Ultraviolet/Visible) model (Madronich and Flocke, 1998).

29 In this study we implement GECKO-A in a similar manner to that described by LT11, with the
30 following modifications. We have implemented the SAR of Vereecken and Peeters (2009) for alkoxy
31 decomposition rates as described in (Aumont et al., 2013), we modified the SAR for hydrogen
32 abstraction from aldehydes, based on the study by (Baker et al., 2004), we added oxy radical
33 production channels for the reactions of R-COO₂ and RO-CH₂O₂ with HO₂ (Orlando and Tyndall, 2012;

1 Hasson et al., 2012), and we updated the branching ratios for isoprene and methacrolein oxidation
2 (Paulot et al., 2009; Galloway et al., 2011).

3 Aerosol condensation in GECKO-A is based on equilibrium partitioning (Pankow, 1994a) assuming
4 unity activity coefficients, and using published vapor pressure (P_{vap}) parameterizations. The model
5 focuses on the gas-particle equilibria of products of gas-phase chemistry with a simple bulk organic
6 aerosol phase which has no aqueous or inorganic component. We prescribe a pre-existing and non-
7 volatile bulk seed aerosol mass to act as a condensation nucleus, as detailed below. We do not
8 consider heterogeneous or particle-phase chemistry, nor any kinetic limitations. Here we employ the
9 vapor pressure scheme of Nannoolal et al. (2008) together with the boiling point scheme of
10 Nannoolal et al. (2004) (together hereinafter NAN), whereas our previous work (LT11) had used the
11 Myrdal and Yalkowsky (1997) vapor pressure scheme which included the boiling point scheme of
12 Joback and Reid (1987) (together hereinafter JRMY). The NAN scheme has been shown to give more
13 realistic (and typically higher) vapor pressure results for longer-chain hydrocarbons than JRMY
14 (Barley and McFiggans, 2010), raising the possibility (examined below) that the aerosol mass
15 production predicted by the JRMY scheme might be an artifact. In the present study we perform a
16 sensitivity study using both methods, to assess how the selection of vapor pressure scheme affects
17 the predicted aerosol mass production.

18 **2.2 Modeling Scenarios**

19 **2.2.1 Urban Precursors: Mexico City during MILAGRO**

20 Our anthropogenic case study is based on the atmosphere in and near Mexico City during the
21 MILAGRO (Megacity Initiative: Local and Global Research Observations) campaign of March 2006
22 (Molina et al., 2010). The emissions and initial conditions are defined similar to LT11, and briefly
23 summarized here. Anthropogenic emissions are a mixture of light aromatics (21% by mass), linear
24 alkanes to C30, (44% by mass, excluding CH4), a selection of branched alkanes to C8 (20% by mass)
25 and alkenes to C6 (12% by mass) (see Figure 1a). Diel cycles of emission rates of chemically-similar
26 groups with up to 10 carbons are specified following Tie et al. (2009). Emissions rates of individual
27 species within the groups are specified according to their observed relative abundances (Apel et al.,
28 2010). Long-chain n-alkanes are used as surrogates for all emitted semi- and intermediate-volatility
29 organic compounds (SVOCs and IVOCs). Their emitted masses are distributed among pre-defined
30 volatility bins as described in LT11. The NAN scheme yields vapor pressures that are progressively
31 higher with increasing carbon number than are those given by JRMY. Hence, the emissions
32 distribution of individual S/IVOCs required to represent the same volatility distribution differs
33 between the two schemes, and was therefore recalculated for NAN in this study. The 9th and lowest

1 volatility bin in the emissions ("SVOC1", centered on $C^* = 1 \times 10^{-2} \mu\text{g m}^{-3}$, where C^* is the effective
2 saturation concentration) corresponds to n-alkane carbon chain lengths of 24-25 under the JRMY
3 scheme but 32-33 for NAN. Precursors in this volatility bin have negligible influence on SOA mass
4 production in LT11, since the ~1% of emitted S/IVOC mass they represent partitions almost
5 exclusively, immediately and irreversibly into the particulate phase as POA. Our current NAN
6 simulations omit emissions from bin SVOC1 to reduce computational load, and specify emissions of
7 n-alkanes up to C30, distributed among 8 volatility bins ranging from 1×10^{-1} to $1 \times 10^6 \mu\text{g m}^{-3}$. The
8 resulting mechanism describes 10.3 million reactions involving almost 1.8 million species and
9 predicts vapor pressures for 0.73 million non-radicals.

10 **2.2.2 Forest Precursors: Manitou Forest during BEACHON**

11 Our biogenic case study is based on Manitou Forest during the BEACHON-ROCS field campaign of
12 summer 2010 (Ortega et al., 2014). The site is dominated by ponderosa pine, giving an ambient VOC
13 mixture high in monoterpenes and low in typical anthropogenic VOCs such as aromatics, alkanes and
14 alkenes. Emissions are represented via mixing-in of air with specified precursor concentrations based
15 on observations (Kaser et al., 2013b). The precursor mix includes selected monoterpenes (α - and β -
16 pinene at 0.11 ppbv each, limonene at 49 pptv, and carene at 29 pptv). Specified oxygenated C1-4
17 species include methyl vinyl ketone at 0.25 ppbv and methyl butenol at 0.78 ppbv. Isoprene, alkanes
18 to C6, alkenes to C5, and aromatics are also included, in the proportions shown in Fig. 1b. Our forest
19 case precursor mixture omits sesquiterpenes because our model has not yet been tested for their
20 complex chemistry. Sesquiterpenes would likely increase the quantity of SOA formed, however we
21 would not expect significant changes to the timing of downwind SOA formation. Like monoterpenes,
22 sesquiterpenes have lifetimes of the order of an hour or less (Atkinson et al., 1990; Shu and
23 Atkinson, 1995). Changing multi-day formation rates would thus require the lifetimes and SOA yields
24 of second or higher -generation sesquiterpene products (Ng et al., 2006) to greatly exceed those for
25 monoterpenes since sesquiterpene source fluxes are relatively low (of the order of 10% or less of
26 monoterpane fluxes during the BEACHON campaign, Kaser et al., 2013a).

27 **2.3 Meteorological conditions and sensitivity studies**

28 Our box model simulations represent photochemical evolution and aerosol condensation in an air
29 parcel that is advected out of a source region and undergoes chemical processing during several
30 days as part of an outflow plume. We initialize the model in the source region, in an Eulerian
31 configuration with diurnally-varying precursor emissions, boundary layer depth, and meteorological
32 conditions. The spin-up period in the urban scenario is driven with meteorological boundary
33 conditions representative of average conditions in Mexico City in March 2006, as in LT11. For

1 biogenic simulations, spin-up meteorological conditions were based on previous regional modeling
2 studies (Cui et al., 2014). Ambient temperatures and boundary layer behavior were similar between
3 the urban and biogenic cases. The spin-up phase lasts for just over 1.5 days, into the early afternoon
4 of our “day 1”. The model simulation then converts into a Lagrangian or outflow period which
5 continues for an additional 3 and 7 days in the forest and urban base cases respectively. Emissions
6 cease and the air parcel (model box) maintains a fixed volume and meteorology and is subject to
7 continuing photochemistry and to dilution with background air. Outflow period meteorological
8 conditions are discussed below.

9 Throughout the model simulations we prescribe a chemically-inert background aerosol, to provide a
10 seed for aerosol condensation. This seed aerosol is intended as a surrogate for regional background
11 aerosol including that produced from local sources and from previous days’ outflow, and contributes
12 to the mass term in the partitioning equation (Pankow, 1994a). Seed aerosol concentration is $2 \mu\text{g m}^{-3}$
13 in the urban case after Hodzic et al. (2009) and Kleinman et al (2008) (corresponding to 6.22×10^9
14 molec cm^{-3} at a molar weight of 200g mol^{-1}), and $1 \mu\text{g m}^{-3}$ for the forest case. Unlike species
15 generated by GECKO-A, the inert seed stays at a constant concentration in the outflow since outflow
16 and background concentrations are equal, hence its relative contribution to the total aerosol mass
17 increases with dilution.

18 For each scenario we perform several sensitivity studies which are initialized with the same Eulerian
19 conditions but diverge at the beginning of the outflow period. Our “base case” simulations continue
20 with constant temperatures of 291K and 288K in the urban and forest scenarios respectively, zero
21 emissions, and a constant e-folding dilution rate k_{dil} of 1 day^{-1} . Outflow conditions begin at 2pm in
22 the forest scenario. In the urban scenario temperature becomes constant and emissions cease at
23 3pm, and the outflow phase begins at 4pm when k_{dil} becomes fixed.

24 In the real world, a plume’s dilution rates and air temperatures are likely to be heterogeneous,
25 varying diurnally as well as with changing plume altitude. However the sensitivity of photochemistry
26 and gas-particle partitioning in a detailed box model to individual environmental variables is most
27 clearly explored by keeping these parameters constant, varying only one at a time. Warmer
28 temperatures should shift the equilibrium towards the gas phase, potentially reducing particle-phase
29 mass (e.g. if aerosol-forming chemical reactions are not temperature sensitive). Our simulation
30 denoted “T+10K” explores the effect on aerosol mass of an outflow temperature increased by 10 K.
31 Plume dilution might also be expected to lead to lower particle mass, since decreasing gas-phase
32 concentrations shift condensation equilibria in favor of evaporation. Simulation “SLOWDIL” is
33 constrained similarly to the base case, however with the outflow-period dilution rate reduced to 0.3
34 day^{-1} in the urban case and 0.46 day^{-1} in the forest case. Simulation “NODIL” uses no dilution at all.

1 Another variable governing the direction of condensation equilibrium is the existing particle mass
2 itself, assuming that Raoult's law applies (Pankow, 1994a). Simulation "SEED/2" reduces seed
3 aerosol mass by 50%, starting from the beginning of the outflow period. Most of our urban outflow
4 simulations inadvertently employed photolysis rates ~20% lower than in LT-11. Rates of
5 photochemical formation and transformation of condensable oxidized products scale with actinic
6 flux, altering the particle mass formation rate. Boundary-layer aerosol pollution reduces actinic flux
7 at the surface but enhances it aloft (Palancar et al, 2013). Simulation "HV+" tests the sensitivity of
8 the particle mass production to increased ambient actinic flux. Effective $j(O1D)$ in case HV+ is about
9 twice that in our urban base case, and about one-third greater than in our forest base case. Finally,
10 simulation "JRMY" is similar to the base case, but with the JRMY vapor pressure scheme, with the
11 S/IVOC emissions adjusted as described above, and with outflow temperatures of 288K. This last
12 sensitivity study was only performed for the urban case. Simulation conditions are summarized in
13 Table 1.

14

15 **3 Results**

16 **3.1 Photochemical Environment**

17 The concentrations of key oxidants simulated within our urban scenario source region have similar
18 profiles to those shown in Figure 3 of LT-11 for Mexico City. (Oxidants are plotted in Figure S.I.1)
19 Peak urban source region concentrations are: $[OH] = 3.2 \times 10^6$ molec cm^{-3} , $[O_3] = 116$ ppbv, and $[NOx]$
20 = 260 ppbv. These values represent highly-polluted urban conditions, where $[OH]$ is suppressed by
21 high $[NOx]$, and are within the range of observations (Dusanter et al., 2009). In the outflow, $[OH]$
22 increases until stabilizing on day 5 at $\sim 8.5 \times 10^6$ molec cm^{-3} . Meanwhile, $[NOx]$ drops rapidly to < 0.8
23 ppbv, and O_3 also declines in response to dilution, to ~ 60 ppbv. The forest case shows oxidant
24 concentrations towards the high end of remote observations (e.g. Wolfe et al, 2014): In the forest
25 outflow $[OH]$ is fairly constant at $\sim 8 \times 10^6$ molec cm^{-3} , $[O_3]$ decreases from 62 to 50 ppbv and NOx
26 falls to consistently low values (~ 0.2 ppbv).

27 The reduced-dilution sensitivity runs demonstrate that net O_3 production continues in the outflow,
28 even as its base case concentrations decrease. In case NODIL, O_3 concentrations increase, weakly in
29 the forest scenario to ~ 70 ppbv on day 4, and strongly in the urban scenario to ~ 175 ppbv on day 5.
30 NODIL NOx is roughly double base case values in both scenarios, which raises forest $[OH]$ levels
31 slightly (to 9×10^6 molec cm^{-3}) but suppresses urban-outflow $[OH]$ to daily maxima of only
32 $\sim 1.3 \times 10^6$ molec cm^{-3} . Case SLOWDIL produces $[O_3]$ and $[NOx]$ levels intermediate between the base
33 and NODIL values, and $[OH]$ similar to NODIL in the urban scenario and similar to base values in the

1 forest scenario. In sensitivity case HV+, urban scenario $[OH]$ is doubled, $[O_3]$ is 50% higher, and
2 afternoon $[NOx]$ 50% lower relative to the base case, while the forest scenario has 30% higher $[OH]$,
3 but largely unaffected $[O_3]$ and $[NOx]$. The urban scenario enhancements continue to high but not
4 unprecedented (Rohrer et al., 2014) peak values of $\sim 17 \times 10^6 \text{ molec cm}^{-3}$, indicating that case HV+
5 provides a good test of the effects on particle mass formation of accelerated gas-phase
6 photochemistry. Sensitivity studies T+10K and SEED/2 have little or no effect on oxidant outflow
7 concentrations.

8 **3.2 Organic aerosol mass production**

9 Figure 2 shows the development of the condensed organic aerosol generated in our set of urban and
10 pine-forest outflow simulations. Lower panels show simulated concentrations and O/C atomic ratios.
11 The spin-up period shows a strong diurnal cycle in response to diel variations in emissions,
12 photolysis, and ventilation. Once the outflow period begins, particle-phase concentrations first peak
13 in response to photochemistry then generally decline in response to dilution. On day 2 (the first full
14 day of outflow), concentrations show an additional photochemistry-induced increase superimposed
15 on the declining baseline, however by day 3 (the second full day of outflow) chemistry-induced
16 concentration changes are barely discernible in either case.

17 To quantify the regional OA mass increase in the expanding plume, which is more relevant to net
18 direct climate effects than is local concentration, we integrate the aerosol concentrations over the
19 entire outflow region. Following LT11, we defined $M_t\text{OA}$ as the organic aerosol mass in a dispersed
20 air parcel with original volume of 1 m^3 , expressed in units of $\mu\text{g initial m}^{-3}$: $M_t\text{OA} = e^{t\cdot k_{\text{dil}}} [OA]_t$ where t
21 is time since the start of the outflow phase. $[OA]_t$ does not include the prescribed constant seed
22 aerosol concentration. Contrary to the progressive decreases in downwind aerosol concentrations,
23 $M_t\text{OA}$ increases throughout the simulation period, although the two base scenarios show very
24 different production rate characteristics from each other. In our urban base case (Fig. 2a), $M_t\text{OA}$
25 increases from $6 \mu\text{g initial m}^{-3}$ at the start of the outflow phase by 140% (to $\sim 14 \mu\text{g initial m}^{-3}$) in the
26 first 24 hours of outflow, and by a factor of >4 (to $26.5 \mu\text{g initial m}^{-3}$) over 4 days. To assess the limits
27 of this production, we continued the simulation for a further 3 days. Particle mass increased
28 asymptotically to a maximum of $28.4 \mu\text{g initial m}^{-3}$ after about a week. Our forest base case (Fig. 2b)
29 also shows particle mass production, although at a far slower rate. $M_t\text{OA}$ begins the outflow phase at
30 $0.8 \mu\text{g m}^{-3}$ and increases by $\sim 60\%$ ($0.5 \mu\text{g initial m}^{-3}$) in the first 24 hours of outflow. Thereafter,
31 however, the production rate slows substantially with $M_t\text{OA}$ rising by only another 5% (to $1.33 \mu\text{g}$
32 initial m^{-3}) during the latter two days of the simulation.

1 Figure 2 also shows particle mass development for our sensitivity simulations. The largest
2 differences in simulated aerosol plume mass are those produced by changing the vapor pressure
3 scheme (performed for the urban case only). Even within the city, JRMY predicts 50% more mid-
4 afternoon aerosol mass than NAN. Downwind, the JRMY case aerosol increases its mass excess over
5 the NAN case, growing by more than a factor of 3 in two days before reaching an asymptote at
6 about 30 $\mu\text{g initial m}^{-3}$ at the end of day 4, slightly sooner than in the NAN case. The initial primary
7 aerosol concentrations are very similar between the two simulations, reflecting the similar volatility
8 distribution of the prescribed emissions. The mass differences arise during SOA production and may
9 be explained by the large differences in estimated P_{vap} for individual species under the two different
10 methods. For example, estimated P_{vap} values for aromatic oxidation products are generally lower by
11 1-3 orders of magnitude under JRMY than under NAN. This allows JRMY to condense SOA with a
12 lesser degree of substitution and at an earlier point in the oxidation process and explains both the
13 early relatively rapid production in the JRMY case, and its earlier slowdown as the available gas
14 phase precursors become depleted. We discuss the chemical composition of the growing aerosol in
15 more detail later. One should not read too much into the slightly higher ending mass of the JRMY
16 aerosol, since this run used lower outflow temperatures. The main result here is that the predicted
17 multiday nature of OA mass production is not unique to one particular vapor pressure scheme. The
18 following discussion refers to simulations performed with the NAN scheme only.

19 The response of the aerosol production rate to environmental conditions is shown in Fig. 2. Particle
20 mass in the outflow plume is rather insensitive to seed aerosol amount, dropping by no more than
21 5% when the seed aerosol is reduced by 50% (runs “SEED/2”). Raising the ambient temperature by
22 10°C (runs “T+10K”) lowers the condensed aerosol mass by between 8 and 25% relative to the base
23 simulation. Increasing the available sunlight (run “HV+”) speeds up initial SOA production. The final
24 condensed aerosol mass is unaffected in the forest scenario, but lower by 9% in the urban scenario,
25 likely owing to increased photolytic removal of semi-volatile gases. In all these sensitivity cases, the
26 aerosol mass reductions noted are insufficient to lead to net mass loss in either the urban or the
27 forest scenario.

28 Slower dilution rates lead to higher aerosol mass concentrations, favoring condensation. In the
29 forest scenario, dilution rate reductions (runs “SLOWDIL” and “NODIL”) give incremental increases in
30 plume-integrated particle mass, as expected. The urban scenario gives a more complex picture.
31 Eliminating dilution entirely (“NODIL”) speeds up initial particle mass production although at longer
32 timescales there is little net mass difference from the base case. However, slowing dilution rates
33 from 1 day^{-1} to 0.3 day^{-1} (run “SLOWDIL”) slows mass production throughout the simulation. This
34 non-monotonic response must result from a combination of factors. In addition to the effect on

1 concentrations noted above, slower dilution leads to continued NOx-suppression of [OH] as noted
2 above, impacting oxidation rates and SOA yields. In addition, SOA yields respond nonlinearly (e.g.
3 Camredon et al., 2007) to [NOx] (which also varies with dilution rate, see earlier). It is likely
4 coincidental that the combinations of conditions in the NODIL and base cases lead to similar SOA
5 mass production. From the point of view of our sensitivity study however, the general result is that
6 particle mass production integrated over the plume is only slightly sensitive to rather radical changes
7 in the dilution rate. This shows that the SOA production is not an artefact of the numerical
8 integration.

9 **3.3 Particle phase chemical composition and properties**

10 The O:C atomic ratio is one of the most widely-used measures of particle chemical composition and
11 degree of oxidation. O:C ratios for the model-generated particle phase in the two base case runs are
12 shown in the lower panels of Fig. 2. Our urban model-generated OA fraction (Fig 2a, lower) shows
13 O:C rising from 0.17 at the start of outflow to 0.42 after 24 hours and 0.71 after 6 days, indicating a
14 particle phase that becomes progressively more oxidized with time. Our forest model-generated OA
15 fraction shows higher O:C ratios throughout (Fig. 2b, lower), developing from 0.84 to 0.90. The
16 differences between the urban and forest scenarios are consistent with the forest case particle
17 phase being already well oxidized at the beginning of the outflow phase, with delayed chemistry in
18 the urban case outflow resulting from [OH] suppression, and with different precursor assemblages
19 giving differently-oxidised products (e.g. Chhabra et al., 2011).

20 O:C values are highly sensitive to the aerosol fraction considered. Our simulations use a pre-existing
21 seed aerosol with a mass concentration of 2 (1) $\mu\text{g m}^{-3}$ in the urban (forest) scenarios respectively.
22 We assign this seed aerosol the same O:C ratio as seen at the end of our forest case (0.9), consistent
23 with a regional background aerosol that is well oxidized and/or of largely biogenic origin (e.g. Hodzic
24 et al. 2010). Including the seed aerosol raises calculated O:C to 0.35 (0.87) at the start of outflow in
25 the urban (forest) cases. The seed aerosol contribution continues to influence the O:C ratio in the
26 outflow, raising urban values to 0.55 after 24 hours and 0.71 after 2.2 days (rather than 7 days).
27 These values are comparable to measurements in Mexico City (0.4-0.73, Aiken et al., 2008; corrected
28 as per Canagaratna et al., 2014), although the strong sensitivity of the O:C ratio to the background
29 aerosol means that model-measurement comparisons are of only limited utility if the background
30 contribution is not known. Our forest scenario values are somewhat higher than measurements
31 during the BEACHON campaign (generally 0.5 - 0.77, Palm et al., 2013), suggesting that our model
32 forest scenario has less anthropogenic influence than does the field data.

1 The chemical composition of organic aerosol may also be expressed in terms of the average
2 molecular weight per carbon (OM:OC), which includes the mass contributions of substituents such as
3 nitrogen. Typical OM:OC values are 1.6 ± 0.2 and 2.1 ± 0.2 for urban and nonurban areas respectively
4 (Turpin and Lim, 2001). OM:OC for our modeled urban outflow aerosol rises from 1.41 to 2.21 over 7
5 days, consistent with a progression from urban to nonurban regimes, while OM:OC in our forest
6 outflow case rises only incrementally, from 2.25 to 2.32, in agreement with the published nonurban
7 values.

8 Examining the evolution of volatility of the particle phase (Fig. 3) shows that particle composition is
9 dynamic in both the urban and forest cases. The particles progressively lose molecules of higher
10 volatility, and gain molecules with lower volatility. The details vary but the net result is that particle
11 phase composition evolves, becoming less volatile with time. This is especially marked in the urban
12 outflow scenario, where the envelope of the volatility distribution shifts to the left by two orders of
13 magnitude.

14 Figure 4 investigates the molecular composition of the simulated particle phase, in terms of carbon
15 number and extent of functionalization. Particles in the urban case (left hand panels) are initially
16 composed mainly of condensed primary emissions (“POA”, species with no functional groups, shown
17 in grey) and SOA formed after one generation of chemistry (species with 1-2 functional groups,
18 shown in red and orange) (Fig. 4a). Figure 4c shows the particle mass distribution after four days of
19 urban outflow. Losses in the grey region centered on C26 show the evaporation of a significant
20 fraction of the primary particle mass. This loss is balanced by a comparable gain in mono- and di-
21 substituted species (red and orange, respectively) with the same carbon numbers, suggesting that
22 the first-generation reaction products of the evaporating primary species are of sufficiently low
23 volatility to partition strongly back to the particle phase. A similar but smaller loss is discernible in
24 the red region around C19, showing re-evaporation also of secondary particle mass. These model
25 results are consistent with measurements by Miracolo et al. (2010) who also found gradual
26 conversion of evaporating POA mass to progressively more oxidized SOA, although on a much
27 shorter time scale in a smog chamber. At lower carbon numbers, mass production occurs after
28 multiple generations of chemistry as shown by the production in species with ≥ 3 functional groups
29 (yellow, green or blue). Indeed, mass gains are found at progressively lower C numbers as time
30 progresses and more highly functionalized products become more abundant. In the forest case (right
31 hand panels) the particle phase shows a relatively high degree of functionalization from the start of
32 the outflow period (Fig. 4b), with most of the contributing species having ≥ 4 functional groups.
33 Again, the particle phase adds more highly functionalized material during the outflow period (Fig.

1 4d) and loses small amounts of less-functionalized material. However, the compositional differences
2 between the early- and late-stage particle phases are much less marked than in the urban case.
3 The long-term particle phase production is much stronger in the urban outflow case than in the
4 forest case, therefore we focus our attention on the urban case with the goal of identifying the
5 compounds that are driving this production. We have already noted that O:C rises throughout the
6 urban outflow simulation. Figure 5 divides the carbon mass in the growing particle phase into
7 fractions based on O:C ratio. The figure shows that the long-term particle mass production is entirely
8 due to more-highly substituted material, with O:C > 0.25. Furthermore, and consistent with Fig. 4,
9 mass-balance considerations show that the majority of this production cannot be explained by the
10 sequence of evaporation, oxidation (possibly including fragmentation) and re-condensation of the
11 less-substituted fractions, since these fractions show comparatively minor losses. The production
12 must therefore be largely due to ongoing incorporation of previously uncondensed material from
13 the gas phase.

14 Figure 6 and Table 2 illustrate the temporal development of gas-particle partitioning for the urban
15 case. The black lines in the Figure represent the carbon mass in each C# bin at the start of the
16 outflow period, with the lower line representing the phase partitioning at that time between particle
17 (below the line) and gas (above the line). The colors of the sub-bars represent the partitioning after 4
18 outflow days. Brown shows particulate carbon, green shows gas phase carbon, and white shows the
19 net carbon loss from each C# bin during the outflow period. Carbon is conserved in our model
20 (numerical losses are of the order of 0.1% per model day). The lost fraction in Fig. 6 and Table 2
21 represents fragmentation which reduces the C# of a molecule, moving carbon to the left and
22 eventually off the figure into species with C# <4. Some general trends are apparent. For the largest,
23 least volatile molecules (C \geq 22) virtually all the carbon partitions to the particle phase, either initially
24 or during the outflow period. Thus, further carbon mass production in this C# range is limited to
25 small increments from evaporation-oxidation-recondensation cycling. The gas phase reservoir is also
26 essentially depleted for the mid-sized molecules (with C# = 10 - 21). However not all the carbon has
27 partitioned into the particle phase, with a substantial portion (up to 60%) removed by
28 fragmentation. Some initial oxidation is usually necessary for fragmentation to occur. The
29 competition between functionalization and fragmentation shifts in favor of increasing fragmentation
30 for molecules with lower C# for two reasons. First, the branching ratio for CO₂ elimination from
31 peroxy acyl radicals increases with decreasing molecular length (Arey et al., 2001; Chacon-Madrid et
32 al., 2010), and second, longer molecules generally have lower volatility so partition earlier to the
33 particle phase where they are protected from further gas-phase reaction (Aumont et al., 2012). For
34 the smaller molecules (C# = 4 – 9) fragmentation is the major fate with only a few percent of the

1 carbon in each bin becoming condensed. However, the much greater burden of these precursors in
2 the outflow means that their contribution to outflow SOA is comparable to that from the mid-sized
3 molecules, and allows substantial particle mass production despite the significant losses to
4 fragmentation. Furthermore, a gas phase carbon reservoir persists in this size range allowing the
5 possibility of further particle mass production, if sufficient functionalization can occur.

6 **3.4 Chemical identity of species responsible for the production**

7 The chemical composition of the gas-particle mixture can be explored in detail uniquely with
8 GECKO-A, because it retains the explicit molecular identity of all intermediates and products. Figure
9 7 shows the time evolution of production rates for different chemical types within the urban outflow
10 particle phase. Production rates fluctuate diurnally in response to photochemistry, showing both a
11 daytime maximum corresponding to the solar-driven cycle in OH and a secondary production peak at
12 sunset originating from nitrate radical chemistry. Mass losses (negative production) also have
13 photochemically-driven diurnal cycles, with aerosol constituents re-volatilizing in response to gas
14 phase removal. The particle phase shows production far exceeding losses for the most abundant
15 individual secondary species and for most groups of similar species.

16 Figure 7 and Table 3 show that a significant proportion of the production in the urban case is
17 attributable to only a few specific chemical species in our mechanism. Of the 20 most abundant
18 individual species (Table 3), three in particular stand out. The fastest-growing single species during
19 daytime is hydroxy-hydroperoxy-maleic anhydride, or “MALANHYOOH”. It is a major product of the
20 oxidation of several different precursors including toluene and α -pinene, and its production rate is
21 roughly correlated with the increasing trend in noontime [OH]. The chemical pathway involves
22 unsaturated γ -dicarbonyl fragmentation products which recyclize to yield maleic anhydride and then
23 undergo addition reactions with OH and HO_2 . This species accounts for about 7% of the particle
24 phase by the simulation end. The fastest-growing species at nightfall is “MNNCATCOOH”, a post-
25 aromatic 4th-generation oxidation product of toluene. It is a peroxide-bicyclic alkene (hereafter
26 denoted “PBA”) with five functional groups: nitrate, nitro, hydroperoxy, and two hydroxy groups. It
27 arises from a sequence of oxidation reactions of toluene culminating in nitrate addition to nitro-di-
28 hydroxy toluene (nitro-catechol), which breaks the aromaticity of the molecule. Its daytime analog,
29 “MNCATECOOH”, is the nitro- hydroperoxide tri-ol, and is the second fastest-growing single species
30 during daytime. Together these three species make up 15% of the particle phase by the end of the
31 simulation. They are also among the most abundant aerosol species in the forest case (Table 4)
32 despite the low abundance of aromatic precursors.

1 Many of the species in Table 3 arise directly from the aromatic mechanism, taken from the MCM
2 rather than from subsequent chemistry generated by SARs from the GECKO-A code. Only the most
3 favorable reaction channel is represented for each oxidation reaction in MCM, raising the possibility
4 of over-representing the relative abundance of an individual product isomer. To address this, in Fig.
5 7a we summarize the behavior of products contained in this portion of the mechanism, *i.e.* those
6 which retain a ring whether aromatic or otherwise. We group these species into classes with similar
7 chemical characteristics and behaviors. Class "(M)MAL" represents the sum of MALANHYOOH and
8 the similar methylated species MMALNHYOOH, which is the ninth-fastest contributor to particle
9 mass production (Table 3). Class "5f-PBN" contains the five-functional PBA nitrates while class "5+4f-
10 PB" represents their daytime analogs and includes a ~20% contribution from the four-functional
11 PBAs. (The mechanism contains no nitrated four-functional PBAs). These two classes also include a
12 minor contribution (<10%) from di-nitro PBAs formed via di-nitro cresols. Together, these three
13 classes (M)MAL, 5f-PBN and 5+4f-PBN account for ~30% of the aerosol mass production during the
14 first 4 days of the urban outflow simulation, and ~40% over 7 days. Furthermore, their relative mass
15 contributions start small (<5% of aerosol mass) but become progressively greater, reaching ~25% of
16 aerosol mass in 4 days and ~30% in 7 days. Other ring-retaining products play little role. Class
17 "aromatics" represents all species retaining aromaticity, including substituted cresols and catechols,
18 which are formed on day 1 but show small net losses from the particle phase over the first 4 days of
19 outflow (~0.2 $\mu\text{g}/\text{initial m}^3$), mainly owing to losses of di-nitro-cresols. The final class in Fig. 7a is
20 "others", encompassing epoxides, quinones, two- and three-functional PBAs, and substituted maleic
21 anhydrides other than the two already described (see also Table 3). This group shows rapid particle-
22 phase mass gains on day 1 in most types of its constituents, followed by largely compensating losses
23 on subsequent days.

24 Particle phase production rates of all other species in the mechanism are plotted in Fig. 7b. POA
25 shows daily net losses, while oxidized species show daily net production peaking around solar noon.
26 We divide the oxidized species into four classes based on carbon number ("C>7" and "C<8") and on
27 whether they include a nitrate or PAN moiety (designated as "N") or not ("noN"). Classes C>7N and
28 C>7noN contribute 33% and 17% respectively to net mass production, while classes C<8N and
29 C<8noN contribute 16% and 5% respectively. Production rates are strong for several days, mainly
30 slowing to zero on or around day 5 with nitrated species showing more sustained production. The
31 larger molecules (C>7), are products of oxidation reactions of aliphatic compounds. Of these, C11-
32 C13 species have the most rapid particle-phase production rates. The smaller molecules (C<8) are
33 products of sequential oxidation and fragmentation reactions of aromatic precursors, with C5
34 species contributing the most production. In terms of chemical identity, the species in these four

1 classes are highly diverse, usually containing at least three different functional groups. Most C<8
2 species with significant production contributions contain at least one PAN or carboxylic acid group,
3 resulting from oxidative addition to a double bond. This is not the case for the major C>7
4 contributors, many of which contain δ -dicarbonyl, δ -hydroxy-hydroperoxy and/or δ -hydroxy-ketone
5 groups resulting from 1,5 hydrogen migration in alkoxy radicals (Orlando et al., 2003). In addition to
6 the daytime production, C<8N species show sustained nighttime production from nitrate and peroxy
7 chemistry.

8 The chemical composition of the urban case particle phase is reflected in the shape of its volatility
9 distribution (Fig. 3a). Figure 8 distributes by half-decade in $\log_{10}(C^*)$ the major chemical classes
10 defined above at the end of the urban simulation. Linear and branched species (classes C>7 and C<8)
11 give an approximately lognormal distribution with respect to $\log_{10}(C^*)$. Superimposed on this base
12 are peaks attributable entirely to products of aromatic chemistry. The largest peak, around $\log_{10}(C^*)$
13 = -1.5 is due to the two substituted maleic anhydrides in class (M)MAL. The secondary peak around
14 $\log_{10}(C^*)$ = -3 results from classes 5f-PBand 5f-PBN. Class 4f-PB is more volatile, giving a small
15 shoulder at $\log_{10}(C^*) \approx -0.5$, while the substituted aromatics produce only a tiny bump in the
16 distribution, around $\log_{10}(C^*)$ = 2.

17 The top 10 species in the forest particle phase are listed in Table 4. The biogenic precursors (a- and
18 b-pinene, and to a lesser extent limonene, isoprene, and carene) give rise to a large variety of
19 condensable oxidation products, as shown by the small mass contributions of even the most
20 abundant species. The maximum individual contribution is only 2.4%, and the top 10 species
21 together account for <14% of the particle mass. The forest case aerosol is highly diverse, with
22 species having both 4- and 6- member rings as well as ring-opened species and fragmentation
23 products. Every species listed contains at least one hydro-peroxy group, reflecting the HO₂-
24 dominant chemistry of this case study. Nitrated species account for about one-third of the mass. The
25 multi-generational product MALANHYOOH appears as the 10th most abundant aerosol species.

26 **4 Discussion and conclusions**

27 Our results show that particle mass production in an outflow plume is a robust feature of our model.
28 The production is largely insensitive to reasonable variations in the seed aerosol amount,
29 temperature, photolysis and dilution rates; rather it appears to be a function of the identity and
30 photo-oxidation pathways of the chemical precursors. In our forest outflow case, high O:C ratios
31 within the plume (Fig. 2) show that the monoterpene precursors are already well oxidized by the
32 time the outflow portion of the simulation begins. While the gas and particle phases continue to be
33 in dynamic equilibrium and the chemical details of their composition evolve over time, there is little

1 change in the total particle mass in the forest case beyond the first few hours of outflow. By
2 contrast, the initial suppression of [OH] in our urban outflow case combined with the longer
3 oxidation lifetimes of the urban precursor mix ensures that the anthropogenic precursor mixture is
4 only partially oxidized. Early increases in modeled urban outflow OA mass are consistent with
5 observations (e.g. Moffett et al., 2010, who found carbon mass increases of >40% per particle over 6
6 hours in the Mexico City plume). The chemistry continues to mature over several days, allowing the
7 total particle mass to grow by a factor of >4 outside the source region. The particle mass production
8 results from multigenerational chemistry operating on gas phase precursors that persist in
9 equilibrium with the particle phase even as the outflow plume dilutes into the surrounding region. In
10 an equilibrium model, particle phase production rates necessarily reflect both gas phase
11 production/loss rates and volatility. As species are depleted in the gas phase, our simulations also
12 show their loss from the particle phase (e.g. in the case of the “other” aromatic compounds in Fig.
13 7). However, in both our urban and forest cases these losses are balanced by fresh condensation of
14 other molecules and/or evaporation-oxidation-condensation processes so that the particle phase
15 volatility distribution shifts to lower vapor pressures and becomes progressively less vulnerable to
16 re-evaporation.

17 Particle-phase mass production in our urban simulation is attributable in roughly equal proportion to
18 oxidation products of light aromatic and long-chain n-alkane precursors. Dodecane has been shown
19 in laboratory photo-oxidation experiments to produce SOA with fourth and higher generation
20 products under low-NO_x conditions (Yee et al., 2012; Craven et al., 2012). These experiments were
21 performed over relatively long timescales (up to 36 hours) and yielded cumulative OH exposures up
22 to about 1×10^8 molec cm⁻³ hr, similar to the 3-day OH exposure experienced by our base case urban
23 aerosol ($\sim 1.5 \times 10^8$ molec cm⁻³ hr). The production in aerosol mass we predict from 4- and 5-functional
24 products of C11-C13 n-alkanes during the first half of our simulation is, therefore, consistent with
25 laboratory results. We use long-chain n-alkanes in this study as surrogates for the wealth of different
26 alkane species emitted in anthropogenic situations (Isaacman et al., 2012; Fraser et al., 1997; Chan
27 et al., 2013). This seems a reasonable approximation since n-alkanes have been shown in several
28 laboratory studies (Lim and Ziemann, 2009a; Yee et al., 2013; Loza et al., 2014) to give SOA yields
29 intermediate between those of branched and of cyclic alkanes, owing to differing OH reaction rates
30 and to the increased (decreased) propensity of branched (cyclic) alkanes to undergo fragmentation.
31 Our model reproduces this behavior (Aumont et al., 2013). Using a more diverse anthropogenic
32 precursor mix from that assumed here could alter the modeled particle-phase production rates and
33 resulting mass, in either direction, but is unlikely to eliminate the production. Therefore these

1 qualifications do not detract from our central result that the particle phase continues to grow for
2 several days downwind of the urban source.

3 We have identified two specific classes of oxidation products of light aromatics, the substituted
4 maleic anhydrides and 5-functional peroxide-bicyclic alkenes (including those with and without
5 nitrate), as major contributors to the SOA production especially in the later days of the simulation.
6 Their delayed influence in the evolving urban outflow is consistent with greater SOA yields from
7 aromatic species under low-NO_x conditions as observed by Chan et al. (2009) and Ng et al. (2007). In
8 the present urban outflow study, these multi-generational products together contribute roughly
9 30% of the particle phase production. Admittedly, our calculations use the NAN vapor pressure
10 scheme far beyond the list of species for which it was validated. However, even if their vapor
11 pressures are underestimated by 1-2 orders of magnitude, these products should be sufficiently
12 involatile to partition strongly to the particle phase (see Fig. 7). We suggest that the substituted
13 maleic anhydrides and 5-functional peroxide-bicyclic alkenes might be useful targets for
14 observational studies seeking to validate our prediction of multiday anthropogenic aerosol
15 production. The fact that only a few species classes contribute such a large proportion of our
16 predicted particle mass production also affects the volatility distribution of the developing aerosol,
17 so that it deviates from a simple lognormal shape. If it can be shown that these species types are
18 indeed important contributors to regional anthropogenic-origin SOA, it will be important to
19 parameterize their volatility distributions for inclusion in regional and global models of aerosol
20 development.

21 Parameterizing SOA formation for routine modeling use is a complex task, and beyond the scope of
22 this paper. Our results can, however, offer some insight. First, and as might be expected, our results
23 illustrate that biogenic, aliphatic anthropogenic, and light-aromatic anthropogenic SOA precursors
24 may be regarded as three distinct classes based on the timescales of resulting SOA mass
25 development and the shapes of the product vapor pressure distributions. Within each of these
26 broad groupings, there is considerable variability of product volatility and chemical characteristics,
27 and GECKO-A has already been used to parameterize correlations for use in 3D models, e.g.,
28 between effective Henry's Law constant and volatility (Hodzic et al., 2013 and 2014), between
29 volatility and mean oxidation state (Aumont et al., 2012) and between carbon number and polarity
30 (Chung et al., 2012). The specific insights given by these studies should contribute to mechanism
31 parameterization efforts.

32 In this study we do not address loss processes that could affect the particle mass in a plume. Explicit
33 chemistry simulations have found dry deposition to be more important than wet deposition (Hodzic
34 et al., 2014). Dry deposition reduces anthropogenic –origin SOA by 15% -40% and biogenic –origin

1 SOA by 40-60% over regionally-relevant timescales, and depending on model conditions and
2 assumed boundary layer depth (Hodzic et al., 2013, Hodzic et al, 2014). Other possible conversion
3 processes include in-particle accretion reactions (Barsanti and Pankow, 2004), heterogeneous
4 oxidation (George and Abbatt, 2010a; Smith et al., 2009; Molina et al., 2004), photolysis (Nizkorodov
5 et al., 2004), and multiphase chemistry (Pun and Seigneur, 2007; Ervens and Volkamer, 2010; Lim
6 and Ziemann, 2009b). These processes which become increasingly important at longer timescales
7 could either increase or decrease particle mass, affect particle hygroscopicity (e.g. George and
8 Abbatt 2010b), and will also likely increase the SOA O:C ratio (e.g. Heald et al, 2010).

9 If our results are generalizable to outflow from anthropogenic sources worldwide, the multiday
10 particle mass production we predict from explicit chemical considerations represents a large but
11 diluting secondary source which is not easily discerned in concentration data. This has implications
12 for the radiative forcing (RF) of climate by anthropogenic organic aerosols. For example, Smith and
13 Bond (2014) recently attributed most RF by organic particles to human-caused biomass burning,
14 with current annual emissions of $17.4 \text{ Tg C yr}^{-1}$. Their assessment relies on the assumption that these
15 OA are purely scattering in the shortwave spectrum, with RF per unit mass comparable to that of
16 sulfate aerosols. Our results, on the other hand, suggest a much larger regional contribution from
17 SOA of urban origin, specifically from the use of fossil fuels comprised in large part of aromatics and
18 long-chain alkanes. The remarkable production shown in Fig. 2(a) would lead to a much larger
19 anthropogenic contribution to the regional - and possibly global - burden of SOA, and their
20 associated RF.

21 A crude estimate shows that large increases in anthropogenic SOA are plausible when viewed
22 together with long-term anthropogenically-driven increases in tropospheric ozone. Northern
23 Hemisphere tropospheric background ozone has increased from pre-industrial values around 10 ppb
24 (Volz and Kley, 1988) to 30-40 ppb (Oltmans et al., 2013). While their precise precursors and
25 formation/removal pathways differ, both tropospheric O_3 and SOA are byproducts of the NOx-
26 catalyzed photo-oxidation of hydrocarbons, and are indeed highly correlated in urban observations.
27 Examples of correlation slopes vary from $30 \mu\text{g m}^{-3} \text{ ppm}^{-1}$ in Houston to $160 \mu\text{g m}^{-3} \text{ ppm}^{-1}$ in Mexico
28 City (e.g. Wood et al., 2010), and application of these slopes to the NH industrial-era increase in
29 background O_3 would correspond to background SOA concentration increases of $0.6\text{-}3.2 \mu\text{g m}^{-3}$. A
30 simple extrapolation over the entire NH in a 1 km PBL implies a hemispheric burden of 0.15-0.8 Tg,
31 and, assuming a 10 day lifetime e.g. (Kristiansen et al., 2012), an annual production rate of 5-30 Tg
32 year^{-1} . Thus it is evident that regional SOA of urban origin have a large potential to modify RF on
33 much larger scales. Unfortunately the optical properties of these SOA particles remain largely
34 unknown; empirical evidence is mounting for strong absorption in the near UV (Kanakidou et al.,

1 2005; Barnard et al., 2008; Lambe et al., 2013) and possibly visible wavelengths as particles age
2 (Updyke et al., 2012), consistent with the presence of complex chromophores such as conjugated
3 carbonyls formed by particle-phase oligomerization (which is not currently represented in our
4 model). The combined uncertainties from the regional production and optical properties of
5 anthropogenic SOA cast some doubt on their current representation in global models.

6 We note also that, in contrast to the anthropogenic SOA, biogenic SOA does not seem to show
7 strong multiday regional production. Given that biogenics represent over 90% of global VOC
8 emissions, even moderate production would have had a large impact on the total SOA budget and
9 would likely yield unrealistically high global SOA concentrations. Anthropogenic VOCs, on the other
10 hand, are shown by our study to have a potentially much larger sphere of influence than previously
11 suspected. Of course we acknowledge many assumptions and approximations inherent in our study,
12 and so we put forward our conclusions tentatively and semi-quantitatively, but with hopefully a
13 clear message that further study is urgently needed to resolve these issues and increase confidence
14 in our understanding of how humans are affecting Earth's climate.

15

16 **Author contributions**

17 J. Lee-Taylor, S. Madronich and A. Hodzic designed the study. J. Lee-Taylor and A. Hodzic performed
18 the simulations. All co-authors contributed to model development. J. Lee-Taylor prepared the
19 manuscript with contributions from all co-authors.

20

21 **Acknowledgements**

22 The National Center for Atmospheric Research is operated by UCAR and sponsored by the National
23 Science Foundation. J. Lee-Taylor was supported by a grant from the U.S. Department of Energy
24 (Office of Science, BER, no. DE-SC0006780) which also partly supported S. Madronich. B. Aumont
25 acknowledges support from the Primequal program of the French Ministry of Ecology, Sustainable
26 Development and Energy, the Sustainable Development Research Network (DIM-R2DS) of the Ile-de-
27 France region and the French ANR within the project ONCEM.

1 References

2 Aiken, A. C., DeCarlo, P. F., Kroll, J. H., Worsnop, D. R., Huffman, J. A., Docherty, K. S., Ulbrich, I. M.,
3 Mohr, C., Kimmel, J. R., Sueper, D., Sun, Y., Zhang, Q., Trimborn, A., Northway, M., Ziemann, P. J.,
4 Canagaratna, M. R., Onasch, T. B., Alfarra, M. R., Prevot, A. S. H., Dommen, J., Duplissy, J., Metzger,
5 A., Baltensperger, U., and Jimenez, J. L.: O/C and OM/OC ratios of primary, secondary, and ambient
6 organic aerosols with highresolution time-of-flight aerosol mass spectrometry, Environ. Sci. Technol.,
7 42, 4478–4485, doi:10.1021/es703009q, 2008.

8 Apel, E. C., Emmons, L. K., Karl, T., Flocke, F., Hills, A. J., Madronich, S., Lee-Taylor, J., Fried, A.,
9 Weibring, P., Walega, J., Richter, D., Tie, X., Mauldin, L., Campos, T., Weinheimer, A., Knapp, D., Sive,
10 B., Kleinman, L., Springston, S., Zaveri, R., Ortega, J., Voss, P., Blake, D., Baker, A., Warneke, C.,
11 Welsh-Bon, D., de Gouw, J., Zheng, J., Zhang, R., Rudolph, J., Junkermann, W., and Riemer, D. D.:
12 Chemical evolution of volatile organic compounds in the outflow of the Mexico City Metropolitan
13 area, Atmos. Chem. Phys., 10, 2353–2375, doi:10.5194/acp-10-2353-2010, 2010.

14 Arey, J., Aschmann, S. M., Kwok, 5 E. S. C., and Atkinson, R.: Alkyl nitrate, hydroxyalkyl nitrate, and
15 hydroxycarbonyl formation from the NO_x-air photooxidations of C-5–C-8 *n*-alkanes, J. Phys. Chem. A,
16 105, 1020–1027, doi:10.1021/jp003292z, 2001.

17 Atkinson, R., Hasegawa, D., and Aschmann, S.M.: Rate constants for the gas-phase reactions of O₃
18 with a series of monoterpenes and related compounds at 296 ± 2 K, Int. J. Chem. Kinetics, 22, 871–
19 887, doi: 10.1002/kin.550220807, 1990.Aumont, B., Szopa, S., and Madronich, S.: Modelling the
20 evolution of organic carbon during its gas-phase tropospheric oxidation: development of an explicit
21 model based on a self generating approach, Atmos. Chem. Phys., 5, 2497–2517, doi:10.5194/acp-5-
22 2497-2005, 2005.

23 Aumont, B., Camredon, M., Valorso, R., Lee-Taylor, J., and Madronich, S.: Development of systematic
24 reduction techniques to describe the SOA/VOC/NO_x/O₃ system, Atmospheric Chemical Mechanisms
25 Conference, 2008.

26 Aumont, B., Valorso, R., Mouchel-Vallon, C., Camredon, M., Lee-Taylor, J., and Madronich, S.:
27 Modeling SOA formation from the oxidation of intermediate volatility *n*-alkanes, Atmos. Chem.
28 Phys., 12, 7577–7589, doi:10.5194/acp-12-7577-2012, 2012.

29 Aumont, B., Camredon, M., Mouchel-Vallon, C., La, S., Ouzebidour, F., Valorso, R., Lee-Taylor, J., and
30 Madronich, S.: Modeling the influence of alkane molecular structure on secondary organic aerosol
31 formation, Faraday Discuss., 165, 105–122, doi:10.1039/c3fd00029j.

1 Baker, J., Arey, J., and Atkinson, R.: Rate constants for the gas-phase reactions of OH radicals with a
2 series of hydroxyaldehydes at 296±2 K, *J. Phys. Chem. A*, 108, 7032–7037, doi:10.1021/jp048979o,
3 2004.

4 Barley, M. H. and McFiggans, G.: The critical assessment of vapour pressure estimation methods for
5 use in modelling the formation of atmospheric organic aerosol, *Atmos. Chem. Phys.*, 10, 749–767,
6 doi:10.5194/acp-10-749-2010, 2010.

7 Barnard, J. C., Volkamer, R., and Kassianov, E. I.: Estimation of the mass absorption cross section of
8 the organic carbon component of aerosols in the Mexico City Metropolitan Area, *Atmos. Chem.*
9 *Phys.*, 8, 6665–6679, doi:10.5194/acp-8-6665-2008, 2008.

10 Barsanti, K. C. and Pankow, J. F.: Thermodynamics of the formation of atmospheric organic
11 particulate matter by accretion reactions – Part 1: aldehydes and ketones, *Atmos. Environ.*, 38,
12 4371–4382, doi:10.1016/j.atmosenv.2004.03.035, 2004.

13 Barsanti, K. C., Carlton, A. G., and Chung, S. H.: Analyzing experimental data and model parameters:
14 implications for predictions of SOA using chemical transport models, *Atmos. Chem. Phys.*, 13,
15 12073–12088, doi:10.5194/acp-13-12073-2013, 2013.

16 Bloss, C., Wagner, V., Bonzanini, A., Jenkin, M. E., Wirtz, K., Martin-Reviejo, M., and Pilling, M. J.:
17 Evaluation of detailed aromatic mechanisms (MCMv3 and MCMv3.1) against environmental
18 chamber data, *Atmos. Chem. Phys.*, 5, 623–639, doi:10.5194/acp-5-623-2005, 2005a.

19 Bloss, C., Wagner, V., Jenkin, M. E., Volkamer, R., Bloss, W. J., Lee, J. D., Heard, D. E., Wirtz, K.,
20 Martin-Reviejo, M., Rea, G., Wenger, J. C., and Pilling, M. J.: Development of a detailed chemical
21 mechanism (MCMv3.1) for the atmospheric oxidation of aromatic hydrocarbons, *Atmos. Chem.*
22 *Phys.*, 5, 641–664, doi:10.5194/acp-5-641-2005, 2005b.

23 Boucher, O., Randall, D., Artaxo, P., Bretherton, C., Feingold, G., Forster, P., Kerminen, V.-M., Kondo,
24 Y., Liao, H., Lohmann, U., Rasch, P., Satheesh, S. K., Sherwood, S., Stevens, B., and Zhan, X. Y.: Clouds
25 and aerosols, in: *Climate Change 2013: The Physical Science Basis, Contribution of Working Group 1*
26 to the Fifth Assessment Report of the IPCC, chap. 7, edited by: Stocker, T. F., Qin, D., Plattner, G.-K.,
27 Tignor, M., Allen, S. K., Boschung, J., Nauels, A., Xia, Y., Bex, V., and Midgley, P. M, Cambridge
28 University Press, Cambridge, UK, and New York, NY, USA, 571–658, 2013.

29 Camredon, M., Aumont, B., Lee-Taylor, J., and Madronich, S.: The SOA/VOC/NO_x system: an explicit
30 model of secondary organic aerosol formation, *Atmos. Chem. Phys.*, 7, 5599–5610, doi:10.5194/acp-
31 7-5599-2007, 2007.

1 Canagaratna, M.R., Jimenez, J.L., Kroll, J.H., Chen, Q., Kessler, S.H., Massoli, P., Hildebrandt Ruiz, L.,
2 Fortner, E., Williams, L.R., Wilson, K.R., Surratt, J.D., Donahue, N.M., Jayne, J.T., and Worsnop, D.R.:
3 Elemental ratio measurements of organic compounds using aerosol mass spectrometry:
4 characterization, improved calibration, and implications, *Atmos. Chem. Phys. Discuss.*, 14, 19791-
5 19835, doi:10.5194/acpd-14-19791-2014, 2014.

6 Carslaw, K. S., Lee, L. A., Reddington, C. L., Mann, G. W., and Pringle, K. J.: The magnitude and
7 sources of uncertainty in global aerosol, *Faraday Discuss.*, 165, 495–512, doi:10.1039/c3fd00043e,
8 2013.

9 Chacon-Madrid, H. J., Presto, A. A., and Donahue, N. M.: Functionalization vs. fragmentation: *n*-
10 aldehyde oxidation mechanisms and secondary organic aerosol formation, *Phys. Chem. Chem. Phys.*,
11 12, 13975–13982, doi:10.1039/c0cp00200c, 2010.

12 Chan, A. W. H., Kautzman, K. E., Chhabra, P. S., Surratt, J. D., Chan, M. N., Crounse, J. D., Kürten, A.,
13 Wennberg, P. O., Flagan, R. C., and Seinfeld, J. H.: Secondary organic aerosol formation from
14 photooxidation of naphthalene and alkynaphthalenes: implications for oxidation of intermediate
15 volatility organic compounds (IVOCs), *Atmos. Chem. Phys.*, 9, 3049–3060, doi:10.5194/acp-9-3049-
16 2009, 2009.

17 Chan, A. W. H., Isaacman, G., Wilson, K. R., Worton, D. R., Ruehl, C. R., Nah, T., Gentner, D. R.,
18 Dallmann, T. R., Kirchstetter, T. W., Harley, R. A., Gilman, J. B., Kuster, W. C., deGouw, J. A.,
19 Offenberg, J. H., Kleindienst, T. E., Lin, Y. H., Rubitschun, C. L., Surratt, J. D., Hayes, P. L., Jimenez, J.
20 L., and Goldstein, A. H.: Detailed chemical characterization of unresolved complex mixtures in
21 atmospheric organics: insights into emission sources, atmospheric processing, and secondary organic
22 aerosol formation, *J. Geophys. Res.-Atmos.*, 118, 6783–6796, doi:10.1002/jgrd.50533, 2013.

23 Chhabra, P. S., Ng, N. L., Canagaratna, M. R., Corrigan, A. L., Russell, L. M., Worsnop, D. R., Flagan, R.
24 C., and Seinfeld, J. H.: Elemental composition and oxidation of chamber organic aerosol, *Atmos.*
25 *Chem. Phys.*, 11, 8827-8845, doi:10.5194/acp-11-8827-2011, 2011. Craven, J. S., Yee, L. D., Ng, N. L.,
26 Canagaratna, M. R., Loza, C. L., Schilling, K. A., Yatavelli, R. L. N., Thornton, J. A., Ziemann, P. J.,
27 Flagan, R. C., and Seinfeld, J. H.: Analysis of secondary organic aerosol formation and aging using
28 positive matrix factorization of high-resolution aerosol mass spectra: application to the dodecane
29 low-NO_x system, *Atmos. Chem. Phys.*, 12, 11795–11817, doi:10.5194/acp-12-11795-2012, 2012.

30 Chung, S. H., Lee-Taylor, J., Asher, W. E., Hodzic, A., Madronich, S., Aumont, B., Pankow, J. F., and
31 Barsanti, K. C., Development of a carbon number polarity grid secondary organic aerosol model with
32 the use of Generator of Explicit Chemistry and Kinetics of Organic in the Atmosphere, poster
33 presented at AGU Fall Meeting, San Francisco, CA, 3-7 December, A53O-0368, 2012.

1 Cui, Y. Y., Hodzic, A., Smith, J. N., Ortega, J., Brioude, J., Matsui, H., Turnipseed, A., Winkler, P., and
2 de Foy, B.: Modeling ultrafine particle growth at a pine forest site influenced by anthropogenic
3 pollution during BEACHON-RoMBAS 2011, *Atmos. Chem. Phys.*, 14, 11011-11-29, doi:10.5194/acp-
4 14-11011-2014, 2014.

5 de Gouw, J. A., Brock, C. A., Atlas, E. L., Bates, T. S., Fehsenfeld, F. C., Goldan, P. D., Holloway, J. S.,
6 Kuster, W. C., Lerner, B. M., Matthew, B. M., Middlebrook, A. M., Onasch, T. B., Peltier, R. E., Quinn,
7 P. K., Senff, C. J., Stohl, A., Sullivan, A. P., Trainer, M., Warneke, C., Weber, R. J., and Williams, E. J.:
8 Sources of particulate matter in the northeastern United States in summer: 1. Direct emissions and
9 secondary formation of organic matter in urban plumes, *J. Geophys. Res.-Atmos.*, 113, D08301,
10 doi:10.1029/2007JD009243, 2008.

11 DeCarlo, P. F., Ulbrich, I. M., Crounse, J., de Foy, B., Dunlea, E. J., Aiken, A. C., Knapp, D., Weinheimer,
12 A. J., Campos, T., Wennberg, P. O., and Jimenez, J. L.: Investigation of the sources and processing of
13 organic aerosol over the Central Mexican Plateau from aircraft measurements during MILAGRO,
14 *Atmos. Chem. Phys.*, 10, 5257–5280, doi:10.5194/acp-10-5257-2010, 2010.

15 Donahue, N. M., Robinson, A. L., Stanier, C. O., and Pandis, S. N.: Coupled partitioning, dilution, and
16 chemical aging of semivolatile organics, *Environ. Sci. Technol.*, 40, 2635–2643,
17 doi:10.1021/es052297c, 2006.

18 Donahue, N. M., Robinson, A. L., and Pandis, S. N.: Atmospheric organic particulate matter: from
19 smoke to secondary organic aerosol, *Atmos. Environ.*, 43, 94–106,
20 doi:10.1016/j.atmosenv.2008.09.055, 2009.

21 Donahue, N. M., Kroll, J. H., Pandis, S. N., and Robinson, A. L.: A two-dimensional volatility basis set –
22 Part 2: Diagnostics of organic-aerosol evolution, *Atmos. Chem. Phys.*, 12, 615– 634, doi:10.5194/acp-
23 12-615-2012, 2012.

24 Dusanter, S., Vimal, D., Stevens, P. S., Volkamer, R., Molina, L. T., Baker, A., Meinardi, S., Blake, D.,
25 Sheehy, P., Merten, A., Zhang, R., Zheng, J., Fortner, E. C., Junkermann, W., Dubey, M., Rahn, T.,
26 Eichinger, B., Lewandowski, P., Prueger, J. and Holder, H.: Measurements of OH and HO₂
27 concentrations during the MCMA-2006 field campaign – Part 2: Model comparison and radical
28 budget, *Atmos. Chem. Phys.*, 9, 6665-6675, doi:10.5194/acp-9-6665-2009, 2009.

29 Dzepina, K., Cappa, C. D., Volkamer, R. M., Madronich, S., DeCarlo, P. F., Zaveri, R. A., and Jimenez, J. L.: Modeling the
30 multiday evolution and aging of secondary organic aerosol during MILAGRO 2006, *Environ. Sci.
31 Technol.*, 45, 3496–3503, doi:10.1021/es103186f, 2011.

1 Ervens, B. and Volkamer, R.: Glyoxal processing by aerosol multiphase chemistry: towards a kinetic
2 modeling framework of secondary organic aerosol formation in aqueous particles, *Atmos. Chem.*
3 *Phys.*, 10, 8219–8244, doi:10.5194/acp-10-8219-2010, 2010.

4 Forster, P., Ramaswamy, V., Artaxo, P., Berntsen, T., Betts, R., Fahey, D. W., Haywood, J., Lean, J.,
5 Lowe, D. C., Myhre, G., Nganga, J., Prinn, R., Raga, G., Schulz, M., and Van Dorland, R.: Changes in
6 atmospheric constituents and in radiative forcing, in: *Climate Change 2007: The Physical Science*
7 *Basis, Contribution of Working Group 1 to the Fourth Assessment Report of the IPCC*, chap. 2, edited
8 by: Solomon, S., Qin, D., Manning, M., Chen, Z., Marquis, M., Averyt, K. B., Tignor, M., and Miller, H.
9 L., Cambridge University Press, Cambridge, UK, and New York, NY, USA, 129–234, 2007.

10 Fraser, M. P., Cass, G. R., Simoneit, B. R. T., and Rasmussen, R. A.: Air quality model evaluation data
11 for organics .4. C-2–C-36 non-aromatic hydrocarbons, *Environ. Sci. Technol.*, 31, 2356–2367, 1997.

12 Galloway, M. M., Huisman, A. J., Yee, L. D., Chan, A. W. H., Loza, C. L., Seinfeld, J. H., and Keutsch, F.
13 N.: Yields of oxidized volatile organic compounds during the OH radical initiated oxidation of
14 isoprene, methyl vinyl ketone, and methacrolein under high-NO_x conditions, *Atmos. Chem. Phys.*,
15 11, 10779–10790, doi:10.5194/acp-11-10779-2011, 2011.

16 George, I. J., and Abbatt, J. P. D.: Heterogeneous oxidation of atmospheric aerosol particles by gas-
17 phase radicals, *Nature Chem.*, 2, 713–722, doi: 10.1038/nchem.806, 2010a.

18 George, I. J., and Abbatt, J. P. D.: Chemical evolution of secondary organic aerosol from OH-initiated
19 heterogeneous oxidation, *Atmos. Chem. Phys.*, 10, 5551–5563, doi: 10.5194/acp-10-5551-2010,
20 2010b.

21 Goldstein, A. H. and Galbally, I. E.: Known and unexplored organic constituents in the earth's
22 atmosphere, *Environ. Sci. Technol.*, 41, 1514–1521, 2007.

23 Grieshop, A. P., Logue, J. M., Donahue, N. M., and Robinson, A. L.: Laboratory investigation of
24 photochemical oxidation of organic aerosol from wood fires 1: measurement and simulation of
25 organic aerosol evolution, *Atmos. Chem. Phys.*, 9, 1263–1277, doi:10.5194/acp-9-1263-2009, 2009.

26 Hallquist, M., Wenger, J. C., Baltensperger, U., Rudich, Y., Simpson, D., Claeys, M., Dommen, J.,
27 Donahue, N. M., George, C., Goldstein, A. H., Hamilton, J. F., Herrmann, H., Hoffmann, T., Iinuma, Y.,
28 Jang, M., Jenkin, M. E., Jimenez, J. L., Kiendler-Scharr, A., Maenhaut, W., McFiggans, G., Mentel, Th.
29 F., Monod, A., Prévôt, A. S. H., Seinfeld, J. H., Surratt, J. D., Szmigielski, R., and Wildt, J.: The
30 formation, properties and impact of secondary organic aerosol: current and emerging issues, *Atmos.*
31 *Chem. Phys.*, 9, 5155–5236, doi:10.5194/acp-9-5155-2009, 2009.

1 Hasson, A. S., Tyndall, G. S., Orlando, J. J., Singh, S., Hernandez, S. Q., Campbell, S., and Ibarra, S. Y.:
2 Branching ratios for the reaction of selected carbonyl-containing peroxy radicals with hydroperoxy
3 radicals, *J. Phys. Chem. A*, 116, 6264–6281, doi:10.1021/jp211799c, 2012.

4 Heald, C. L., Kroll, J. H., Jimenez, J. O., Docherty, K. S., DeCarlo, P. F., Aiken, A. C., Chen, Q., Martin, S.
5 T., Farmer, D. K., and Artaxo, P.: A simplified description of the evolution of organic aerosol
6 composition in the atmosphere, *Geophys. Res. Lett.*, 37, L08803, doi: 10.1029/2010GL042737, 2010.

7 Heald, C. L., Coe, H., Jimenez, J. L., Weber, R. J., Bahreini, R., Middlebrook, A. M., Russell, L. M.,
8 Jolleys, M., Fu, T.-M., Allan, J. D., Bower, K. N., Capes, G., Crosier, J., Morgan, W. T., Robinson, N. H.,
9 Williams, P. I., Cubison, M. J., DeCarlo, P. F., and Dunlea, E. J.: Exploring the vertical profile of
10 atmospheric organic aerosol: comparing 17 aircraft field campaigns with a global model, *Atmos.*
11 *Chem. Phys.*, 11, 12673–12696, doi:10.5194/acp-11-12673-2011, 2011.

12 Hodzic, A., Jimenez, J. L., Madronich, S., Aiken, A. C., Bessagnet, B., Curci, G., Fast, J., Lamarque, J.-F.,
13 Onasch, T. B., Roux, G., Schauer, J. J., Stone, E. A., and Ulbrich, I. M.: Modeling organic aerosols
14 during MILAGRO: importance of biogenic secondary organic aerosols, *Atmos. Chem. Phys.*, 9, 6949–
15 6981, doi:10.5194/acp-9-6949-2009, 2009.

16 Hodzic, A., Jimenez, J. L., Prévôt, A. S. H., Szidat, S., Fast, J. D., and Madronich, S.: Can 3-D models
17 explain the observed fractions of fossil and non-fossil carbon in and near Mexico City? *Atmos. Chem.*
18 *Phys.*, 10, 10997-11016, doi:10.5194/acp-10-10997-2010, 2010.

19 Hodzic, A., Madronich, S., Aumont, B., Lee-Taylor, J., Karl, T., Camredon, M., and Mouchel-Vallon, C.:
20 Limited influence of dry deposition of semivolatile organic vapors on secondary organic aerosol
21 formation in the urban plume, *Geophys. Res. Lett.*, 40, 3302–3307, doi:10.1002/grl.50611, 2013.

22 Hodzic, A., Aumont, B., Knot, C., Lee-Taylor, J., Madronich, S., and Tyndall, G.: Volatility dependence
23 of Henry's law constants of condensable organics: Application to estimate depositional loss of
24 secondary organic aerosols, *Geophys. Res. Lett.*, 41, 4795–4804, doi: 10.1002/2014GL060649, 2014.

25 Isaacman, G., Chan, A. W. H., Nah, T., Worton, D. R., Ruehl, C. R., Wilson, K. R., and Goldstein, A. H.:
26 Heterogeneous OH oxidation of motor oil particles causes selective depletion of branched and less
27 cyclic hydrocarbons, *Environ. Sci. Technol.*, 46, 10632–10640, 25 doi:10.1021/es302768a, 2012.

28 Jenkin, M. E., Saunders, S. M., Wagner, V., and Pilling, M. J.: Protocol for the development of the
29 Master Chemical Mechanism, MCM v3 (Part B): tropospheric degradation of aromatic volatile
30 organic compounds, *Atmos. Chem. Phys.*, 3, 181–193, doi:10.5194/acp-3-181-2003, 2003.

31 Jimenez, J. L., Canagaratna, M. R., Donahue, N. M., Prevot, A. S. H., Zhang, Q., Kroll, J. H., DeCarlo, P.
32 F., Allan, J. D., Coe, H., Ng, N. L., Aiken, A. C., Docherty, K. S., Ulbrich, I. M., Grieshop, A. P., Robinson,

1 A. L., Duplissy, J., Smith, J. D., Wilson, K. R., Lanz, V. A., Hueglin, C., Sun, Y. L., Tian, J., Laaksonen, A.,
2 Raatikainen, T., Rautiainen, J., Vaattovaara, P., Ehn, M., Kulmala, M., Tomlinson, J. M., Collins, D. R.,
3 Cubison, M. J., Dunlea, E. J., Huffman, J. A., Onasch, T. B., Alfarra, M. R., Williams, P. I., Bower, K.,
4 Kondo, Y., Schneider, J., Drewnick, F., Borrmann, S., Weimer, S., Demerjian, K., Salcedo, D., Cottrell,
5 L., Griffin, R., Takami, A., Miyoshi, T., Hatakeyama, S., Shimono, A., Sun, J. Y., Zhang, Y. M., Dzepina,
6 K., Kimmel, J. R., Sueper, D., Jayne, J. T., Herndon, S. C., Trimborn, A. M., Williams, L. R., Wood, E.
7 C., Middlebrook, A. M., Kolb, C. E., Baltensperger, U., and Worsnop, D. R.: Evolution of organic
8 aerosols in the atmosphere, *Science*, 326, 1525–1529, doi:10.1126/science.1180353, 2009.

9 Jo, D. S., Park, R. J., Kim, M. J., and Spracklen, D. V.: Effects of chemical aging on global secondary
10 organic aerosol using the volatility basis set approach, *Atmos. Environ.*, 81, 230–244,
11 doi:10.1016/j.atmosenv.2013.08.055, 2013.

12 Joback, K. G. and Reid, R. C.: Estimation of pure-component properties from groupcontribution, *Chem. Eng. Commun.*, 57, 233–243, 1987.

14 Kanakidou, M., Seinfeld, J. H., Pandis, S. N., Barnes, I., Dentener, F. J., Facchini, M. C., Van Dingenen,
15 R., Ervens, B., Nenes, A., Nielsen, C. J., Swietlicki, E., Putaud, J. P., Balkanski, Y., Fuzzi, S., Horth, J.,
16 Moortgat, G. K., Winterhalter, R., Myhre, C. E. L., Tsigaridis, K., Vignati, E., Stephanou, E. G., and
17 Wilson, J.: Organic aerosol and global climate modelling: a review, *Atmos. Chem. Phys.*, 5, 1053–
18 1123, doi:10.5194/acp-5-1053-2005, 2005.

19 Kaser, L., Karl, T., Guenther, A., Graus, M., Schnitzhofer, R., Turnipseed, A., Fischer, L., Harley, P.,
20 Madronich, M., Gochis, D., Keutsch, F. N., and Hansel, A.: Undisturbed and disturbed above canopy
21 ponderosa pine emissions: PTR-TOF-MS measurements and MEGAN 2.1 model results, *Atmos.*
22 *Chem. Phys.*, 13, 11935–11947, doi:10.5194/acp-13-11935-2013, 2013a.

23 Kaser, L., Karl, T., Schnitzhofer, R., Graus, M., Herdlinger-Blatt, I. S., DiGangi, J. P., Sive, B.,
24 Turnipseed, A., Hornbrook, R. S., Zheng, W., Flocke, F. M., Guenther, A., Keutsch, F. N., Apel, E., and
25 Hansel, A.: Comparison of different real time VOC measurement techniques in a ponderosa pine
26 forest, *Atmos. Chem. Phys.*, 13, 2893–2906, doi:10.5194/acp-13-2893-2013, 2013b.

27 Kleinman, L. I., Springston, S. R., Daum, P. H., Lee, Y. -N., Nunnermacker, L. J., Senum, G. I., Wang, J.,
28 Weinstein-Lloyd, J., Alexander, M. L., Hubbe, Ortega, J., Canagaratna, M. R., and Jayne, J.: The time
29 evolution of aerosol composition over the Mexico City plateau, *Atmos. Chem. Phys.*, 8, 1559–1575,
30 doi:10.5194/acp-8-1559-2008, 2008.

31 Kourtchev, I., Connoer, I. P., Giorio, C., Fuller, S. J., Kristensen, K., Maenhaut, W., Wenger, J. C., Sodeau,
32 J. R., Glasius, M., Kalberer, M.: Effects of anthropogenic emissions on the molecular composition of

1 urban organic aerosols: An ultrahigh resolution mass spectrometry study, *Atmos. Environ.*, 89, 525-
2 532, doi:10.1016/j.atmosenv.2014.02.051, 2014.

3 Kristiansen, N. I., Stohl, A., and Wotawa, G.: Atmospheric removal times of the aerosol-bound
4 radionuclides ^{137}Cs and ^{131}I measured after the Fukushima Dai-ichi nuclear accident – a constraint
5 for air quality and climate models, *Atmos. Chem. Phys.*, 12, 10759–10769, doi:10.5194/acp-12-
6 10759-2012, 2012.

7 Kroll, J. H. and Seinfeld, J. H.: Chemistry of secondary organic aerosol: formation and evolution of
8 low-volatility organics in the atmosphere, *Atmos. Environ.*, 42, 3593–3624, 30
9 doi:10.1016/j.atmosenv.2008.01.003, 2008.

10 Kroll, J. H., Donahue, N. M., Jimenez, J. L., Kessler, S. H., Canagaratna, M. R., Wilson, K. R., Altieri, K.
11 E., Mazzoleni, L. R., Wozniak, A. S., Bluhm, H., Mysak, E. R., Smith, J. D., Kolb, C. E., and Worsnop, D.
12 R.: Carbon oxidation state as a metric for describing the chemistry of atmospheric organic aerosol,
13 *Nature Chemistry*, 3, 133–139, doi:10.1038/NCHEM.948, 2011.

14 Lambe, A. T., Cappa, C. D., Massoli, P., Onasch, T. B., Forestieri, S. D., Martin, A. T., Cummings, M. J.,
15 Croasdale, D. R., Brune, W. H., Worsnop, D. R., and Davidovits, P.: Relationship between oxidation
16 level and optical properties of secondary organic aerosol, *Environ. Sci. Technol.*, 47, 6349–6357,
17 doi:10.1021/es401043j, 2013.

18 Lane, T. E., Donahue, N. M., and Pandis, S. N.: Simulating secondary organic aerosol formation using
19 the volatility basis-set approach in a chemical transport model, *Atmos. Environ.*, 42, 7439–7451,
20 doi:10.1016/j.atmosenv.2008.06.026, 2008.

21 Lee-Taylor, J., Madronich, S., Aumont, B., Baker, A., Camredon, M., Hodzic, A., Tyndall, G. S., Apel, E.,
22 and Zaveri, R. A.: Explicit modeling of organic chemistry and secondary organic aerosol partitioning
23 for Mexico City and its outflow plume, *Atmos. Chem. Phys.*, 11, 13219–13241, doi:10.5194/acp-11-
24 13219-2011, 2011.

25 Lim, Y. B. and Ziemann, P. J.: Effects of molecular structure on aerosol yields from OH radical-
26 initiated reactions of linear, branched, and cyclic alkanes in the presence of NO_x, *Environ. Sci.*
27 *Technol.*, 43, 2328–2334, doi:10.1021/es803389s, 2009a.

28 Lim, Y. B. and Ziemann, P. J.: Kinetics of the heterogeneous conversion of 1,4-hydroxycarbonyls to
29 cyclic hemiacetals and dihydrofurans on organic aerosol particles, *Phys. Chem. Chem. Phys.*, 11,
30 8029–8039, doi:10.1021/es803389s, 2009b.

1 Lin, G., Penner, J. E., Sillman, S., Taraborrelli, D., and Lelieveld, J.: Global modeling of SOA formation
2 from dicarbonyls, epoxides, organic nitrates and peroxides, *Atmos. Chem. Phys.*, 12, 4743–4774,
3 doi:10.5194/acp-12-4743-2012, 2012.

4 Loza, C. L., Craven, J. S., Yee, L. D., Coggon, M. M., Schwantes, R. H., Shiraiwa, M., Zhang, X., Schilling,
5 K. A., Ng, N. L., Canagaratna, M. R., Ziemann, P. J., Flagan, R. C., and Seinfeld, J. H.: Secondary organic
6 aerosol yields of 12-carbon alkanes, *Atmos. Chem. Phys.*, 14, 1423–1439, doi:10.5194/acp-14-1423-
7 2014, 2014.

8 Madronich, S., and Flocke, S.: The role of solar radiation in atmospheric chemistry, Chap 1 in
9 *Handbook of Environmental Chemistry*, edited by Boule, P., Springer-Verlag, New York, NY. USA, 1-
10 26, 1998.

11 Mahmud, A. and Barsanti, K.: Improving the representation of secondary organic aerosol (SOA) in
12 the MOZART-4 global chemical transport model, *Geosci. Model Dev.*, 6, 961–980, doi:10.5194/gmd-
13 6-961-2013, 2013.

14 McFiggans, G., Artaxo, P., Baltensperger, U., Coe, H., Facchini, M. C., Feingold, G., Fuzzi, S., Gysel, M.,
15 Laaksonen, A., Lohmann, U., Mentel, T. F., Murphy, D. M., O'Dowd, C. D., Snider, J. R., and
16 Weingartner, E.: The effect of physical and chemical aerosol properties on warm cloud droplet
17 activation, *Atmos. Chem. Phys.*, 6, 2593–2649, doi:10.5194/acp-6-2593-2006, 2006.

18 Miracolo, M. A., Presto, A. A., Lambe, A. T., Hennigan, C. J., Donahue, N. M., Kroll, J. H., Worsnop, D.
19 R., and Robinson, A. L.: Photo-oxidation of low-volatility organics found in motor 5 vehicle emissions:
20 production and chemical evolution of organic aerosol mass, *Environ. Sci. Technol.*, 44, 1638–1643,
21 doi:10.1021/es902635c, 2010.

22 Moffet, R. C., Henn, T. R., Tivanski, A. V., Hopkins, R. J., Desyaterik, Y., Kilcoyne, A. L. D., Tyliszczak, T.,
23 Fast, J., Barnard, J., Shutthanandan, V., Cliff, S. S., Perry, K. D., Laskin, A., and Gilles, M. K.:
24 Microscopic characterization of carbonaceous aerosol particle aging in the outflow from Mexico City,
25 *Atmos. Chem. Phys.*, 10, 961-976, doi:10.5194/acp-10-961-2010, 2010.

26 Molina, L. T., Madronich, S., Gaffney, J. S., Apel, E., de Foy, B., Fast, J., Ferrare, R., Herndon, S.,
27 Jimenez, J. L., Lamb, B., Osornio-Vargas, A. R., Russell, P., Schauer, J. J., Stevens, P. S., Volkamer, R.,
28 and Zavala, M.: An overview of the MILAGRO 2006 Campaign: Mexico City emissions and their
29 transport and transformation, *Atmos. Chem. Phys.*, 10, 8697–8760, doi:10.5194/acp-10-8697-2010,
30 2010.

31 Molina, M. J., Ivanov, A. V., Trakhtenberg, S., and Molina, L. T.: Atmospheric evolution of organic
32 aerosol, *Geophys. Res. Lett.*, 31, , L22104, doi:10.1029/2004gl020910, 2004.

1 Murphy, B. N., Donahue, N. M., Fountoukis, C., Dall’Osto, M., O’Dowd, C., Kiendler-Scharr, A., and
2 Pandis, S. N.: Functionalization and fragmentation during ambient organic aerosol aging: application
3 of the 2-D volatility basis set to field studies, *Atmos. Chem. Phys.*, 12, 10797–10816,
4 doi:10.5194/acp-12-10797-2012, 2012.

5 Myhre, G., Samset, B. H., Schulz, M., Balkanski, Y., Bauer, S., Berntsen, T. K., Bian, H., Bellouin, N.,
6 Chin, M., Diehl, T., Easter, R. C., Feichter, J., Ghan, S. J., Hauglustaine, D., Iversen, T., Kinne, S.,
7 Kirkevåg, A., Lamarque, J.-F., Lin, G., Liu, X., Lund, M. T., Luo, G., Ma, X., van Noije, T., Penner, J. E.,
8 Rasch, P. J., Ruiz, A., Seland, Ø., Skeie, R. B., Stier, P., Takemura, T., Tsigaridis, K., Wang, P., Wang, Z.,
9 Xu, L., Yu, H., Yu, F., Yoon, J.-H., Zhang, K., Zhang, H., and Zhou, C.: Radiative forcing of the direct
10 aerosol effect from AeroCom Phase II simulations, *Atmos. Chem. Phys.*, 13, 1853–1877,
11 doi:10.5194/acp-13-1853-2013, 2013.

12 Myrdal, P. B. and Yalkowsky, S. H.: Estimating pure component vapor pressures of complex organic
13 molecules, *Ind. Eng. Chem. Res.*, 36, 2494–2499, 1997.

14 Nannoolal, Y., Rarey, J., Ramjugernath, D., and Cordes, W.: Estimation of pure component properties
15 – Part 1. Estimation of the normal boiling point of non-electrolyte organic compounds via group
16 contributions and group interactions, *Fluid Phase Equilibr.*, 226, 45–63, 30 2004.

17 Nannoolal, Y., Rarey, J., and Ramjugernath, D.: Estimation of pure component properties – Part 3.
18 Estimation of the vapor pressure of non-electrolyte organic compounds via group contributions and
19 group interactions, *Fluid Phase Equilibr.*, 269, 117–133, 2008.

20 Ng, N.L., Kroll, J.H., Keywood, M.D., Bahreini, R., Varutbangkul, V., Flagan, R.C., Seinfeld, J.H., Lee, A.,
21 and Goldstein, A.H.: Contribution of First- versus Second-Generation Products to Secondary Organic
22 Aerosols Formed in the Oxidation of Biogenic Hydrocarbons, *Environ. Sci. Technol.*, 40, 2283–2297,
23 doi: 10.1021/es052269u, 2006.

24 Ng, N. L., Kroll, J. H., Chan, A. W. H., Chhabra, P. S., Flagan, R. C., and Seinfeld, J. H.: Secondary
25 organic aerosol formation from *m*-xylene, toluene, and benzene, *Atmos. Chem. Phys.*, 7, 3909–3922,
26 doi:10.5194/acp-7-3909-2007, 2007.

27 Nizkorodov, S., Gomez, A., Lin, A., Whitt, D., and Alshawa, A.: Photodissociation action spectroscopy
28 at 5 organic aerosol particle–air interfaces, *Abstr. Pap. Am. Chem. S.*, 228, U226–U226, 2004.

29 Nizkorodov, S.A., Laskin, J. and Laskin, A.: Molecular chemistry of organic aerosols through the
30 application of high resolution mass spectrometry, *Phys. Chem. Chem. Phys.*, 13, 3612-3629, doi:
31 10.1039/C0CP02032J, 2011.

1 Odum, J. R., Hoffmann, T., Bowman, F., Collins, D., Flagan, R. C., and Seinfeld, J. H.: Gas/particle
2 partitioning and secondary organic aerosol yields, *Environ. Sci. Technol.*, 30, 2580–2585, 1996.

3 Oltmans, S. J., Lefohn, A. S., Shadwick, D., Harris, J. M., Scheel, H. E., Galbally, I., Tarasick, D. W.,
4 Johnson, B. J., Brunke, E. G., Claude, H., Zeng, G., Nichol, S., Schmidlin, F., Davies, J., Cuevas, E.,
5 Redondas, A., Naoe, H., Nakano, T., and Kawasato, T.: Recent tropospheric ozone changes – a
6 pattern dominated by slow or no growth, *Atmos. Environ.*, 67, 331–351,
7 doi:10.1016/j.atmosenv.2012.10.057, 2013.

8 Orlando, J. J. and Tyndall, G. S.: Laboratory studies of organic peroxy radical chemistry: an overview
9 with emphasis on recent issues of atmospheric significance, *Chem. Soc. Rev.*, 41, 6294–6317,
10 doi:10.1039/c2cs35166h, 2012.

11 Orlando, J. J., Tyndall, G. S., and Wallington, T. J.: The atmospheric chemistry of alkoxy radicals,
12 *Chem. Rev.*, 103, 4657–4689, doi:10.1021/cr020527p, 2003.

13 Ortega, J., Turnipseed, A., Guenther, A. B., Karl, T. G., Day, D. A., Gochis, D., Huffman, J. A., Prenni, A.
14 J., Levin, E. J. T., Kreidenweis, S. M., DeMott, P. J., Tobo, Y., Patton, E. G., Hodzic, A., Cui, Y. Y., Harley,
15 P. C., Hornbrook, R. S., Apel, E. C., Monson, R. K., Eller, A. S. D., Greenberg, J. P., Barth, M. C.,
16 Campuzano-Jost, P., Palm, B. B., Jimenez, J. L., Aiken, A. C., Dubey, M. K., Geron, C., Offenberg, J.,
17 Ryan, M. G., Fornwalt, P. J., Pryor, S. C., Keutsch, F. N., DiGangi, J. P., Chan, A. W. H., Goldstein, A. H.,
18 Wolfe, G. M., Kim, S., Kaser, L., Schnitzhofer, R., Hansel, A., Cantrell, C. A., Mauldin, R. L., and Smith,
19 J. N.: Overview of the Manitou Experimental Forest Observatory: site description and selected
20 science results from 2008 to 2013, *Atmos. Chem. Phys.*, 14, 6345–6367, doi:10.5194/acp-14-6345-
21 2014, 2014.

22 Palancar, G.G., Lefer, B.J., Hall, S.R., Shaw, W.J., Corr, C.A., Herndon, S.C., Slusser, J.R., and
23 Madronich, S.: Effect of aerosols and NO₂ concentration on ultraviolet actinic flux near Mexico City
24 during MILAGRO: measurements and model calculations, *Atmos. Chem. Phys.*, 13, 1011-1022,
25 doi:10.5194/acp-13-1011-2013, 2013.

26 Palm, B. B., Ortega, A. M., Campuzano Jost, P., Day, D. A., Fry, J., Zarzana, K. J., Draper, D. C., Brown,
27 S. S., Kaser, L., Karl, T., Jud, W., Hansel, A., Hodzic, A., Dube, W. P., Wagner, N. L., Brune, W. H., and
28 Jimenez, J. L.: Characterizing the Amount and Chemistry of Biogenic SOA Formation from Pine Forest
29 Air Using a Flow Reactor, poster presented at AGU Fall Meeting, San Francisco, CA, 9–13 December,
30 A13B–0187, 2013.

31 Pankow, J. F.: An absorption-model of gas-particle partitioning of organic-compounds in the
32 atmosphere, *Atmos. Environ.*, 28, 185–188, doi:10.1016/1352-2310(94)90093-0, 1994a.

1 Pankow, J. F.: An absorption-model of the gas aerosol partitioning involved in the formation of
2 secondary organic aerosol, *Atmos. Environ.*, 28, 189–193, doi:10.1016/1352-5 2310(94)90094-9,
3 1994b.

4 Pankow, J. F. and Barsanti, K. C.: The carbon-number-polarity grid: a means to manage
5 the complexity of the mix of organic compounds when modeling atmospheric organic particulate
6 matter, *Atmos. Environ.*, 43, 2829–2835, 2009. Paulot, F., Crounse, J. D., Kjaergaard, H. G., Kroll, J. H.,
7 Seinfeld, J. H., and Wennberg, P. O.: Isoprene photooxidation: new insights into the production of
8 acids and organic nitrates, *Atmos. Chem. Phys.*, 9, 1479–1501, doi:10.5194/acp-9-1479-2009, 2009.

9 Pun, B. K. and Seigneur, C.: Investigative modeling of new pathways for secondary organic aerosol
10 formation, *Atmos. Chem. Phys.*, 7, 2199–2216, doi:10.5194/acp-7-2199-2007, 2007.

11 Pye, H. O. T. and Pouliot, G. A.: Modeling the role of alkanes, polycyclic aromatic hydrocarbons, and
12 their oligomers in secondary organic aerosol formation, *Environ. Sci. Technol.*, 46, 6041–6047,
13 doi:10.1021/es300409w, 2012.

14 Robinson, A. L., Donahue, N. M., Shrivastava, M. K., Weitkamp, E. A., Sage, A. M., Grieshop, A. P.,
15 Lane, T. E., Pierce, J. R., and Pandis, S. N.: Rethinking organic aerosols: semivolatile emissions and
16 photochemical aging, *Science*, 315, 1259–1262, doi:10.1126/science.1133061, 2007.

17 Rohrer, F., Lu, K., Hofzumahaus, A., Born, B., Brauers, T., Chang, C.-C., Fuchs, H., Häseler, R., Holland,
18 F., Hu, M., Kita, K., Kondo, Y., Li, X., Lou, S., Oebel, A., Shao, M., Zeng, L., Zhu, T., Zhang, Y., and
19 Wahner, A.: Maximum efficiency in the hydroxyl-based self-cleansing of the troposphere, *Nature
20 Geoscience*, 7, doi:10.1038/NGEO2199, 2014.

21 Shu, Y., and Atkinson, R.: Atmospheric lifetimes and fates of a series of sesquiterpenes, *J. Geophys.
22 Res*, 100, 7275–7281, doi: 10.1029/95JD00368, 1995. Smith, J. D., Kroll, J. H., Cappa, C. D., Che, D. L.,
23 Liu, C. L., Ahmed, M., Leone, S. R., Worsnop, D. R., and Wilson, K. R.: The heterogeneous reaction of
24 hydroxyl radicals with sub-micron squalane particles: a model system for understanding the
25 oxidative aging of ambient aerosols, *Atmos. Chem. Phys.*, 9, 3209–3222, doi:10.5194/acp-9-3209-
26 2009, 2009.

27 Smith, S. J. and Bond, T. C.: Two hundred fifty years of aerosols and climate: the end of the age of
28 aerosols, *Atmos. Chem. Phys.*, 14, 537–549, doi:10.5194/acp-14-537-2014, 2014.

29 Spracklen, D. V., Jimenez, J. L., Carslaw, K. S., Worsnop, D. R., Evans, M. J., Mann, G. W., Zhang, Q.,
30 Canagaratna, M. R., Allan, J., Coe, H., McFiggans, G., Rap, A., and Forster, P.: Aerosol mass
31 spectrometer constraint on the global secondary organic aerosol budget, *Atmos. Chem. Phys.*, 11,
32 12109–12136, doi:10.5194/acp-11-12109-2011, 2011.

1 Stockwell, W. R., Kirchner, F., Kuhn, M., and Seefeld, S.: A new mechanism for regional atmospheric
2 chemistry modeling, *J. Geophys. Res.-Atmos.*, 22, 25847–25879, 1997.

3 Szopa, S., Aumont, B., and Madronich, S.: Assessment of the reduction methods used to develop
4 chemical schemes: building of a new chemical scheme for VOC oxidation suited to three-dimensional
5 multiscale HOx–NOx–VOC chemistry simulations, *Atmos. Chem. Phys.*, 5, 2519–2538,
6 doi:10.5194/acp-5-2519-2005, 2005.

7 Tie, X., Madronich, S., Li, G., Ying, Z., Weinheimer, A., Apel, E., and Campos, T.: Simulation of
8 Mexico City plumes during the MIRAGE-Mex field campaign using the WRF-Chem model, *Atmos.*
9 *Chem. Phys.*, 9, 4621–4638, doi:10.5194/acp-9-4621-2009, 2009.

10 Trivitayanurak, W. and Adams, P. J.: Does the POA–SOA split matter for global CCN formation?,
11 *Atmos. Chem. Phys.*, 14, 995–1010, doi:10.5194/acp-14-995-2014, 2014.

12 Tsigaridis, K., Daskalakis, N., Kanakidou, M., Adams, P. J., Artaxo, P., Bahadur, R., Balkanski, Y., Bauer,
13 S. E., Bellouin, N., Benedetti, A., Bergman, T., Berntsen, T. K., Beukes, J. P., Bian, H., Carslaw, K. S.,
14 Chin, M., Curci, G., Diehl, T., Easter, R. C., Ghan, S. J., Gong, S. L., Hodzic, A., Hoyle, C. R., Iversen, T.,
15 Jathar, S., Jimenez, J. L., Kaiser, J. W., Kirkevåg, A., Koch, D., Kokkola, H., Lee, Y. H., Lin, G., Liu, X.,
16 Luo, G., Ma, X., Mann, G. W., Mihalopoulos, N., Morcrette, J.-J., Müller, J.-F., Myhre, G.,
17 Myrookefalitakis, S., Ng, S., O'Donnell, D., Penner, J. E., Pozzoli, L., Pringle, K. J., Russell, L. M., Schulz,
18 M., Sciare, J., Seland, Ø., Shindell, D. T., Sillman, S., Skeie, R. B., Spracklen, D., Stavrakou, T.,
19 Steenrod, S. D., Takemura, T., Tiitta, P., Tilmes, S., Tost, H., van Noije, T., van Zyl, P. G., von Salzen, K.,
20 Yu, F., Wang, Z., Wang, Z., Zaveri, R. A., Zhang, H., Zhang, K., Zhang, Q., and Zhang, X.: The AeroCom
21 evaluation and intercomparison of organic aerosol in global models, *Atmos. Chem. Phys.*, 14, 10845–
22 10895, doi:10.5194/acp-14-10845-2014, 2014.

23 Tsimpidi, A. P., Karydis, V. A., Zavala, M., Lei, W., Molina, L., Ulbrich, I. M., Jimenez, J. L., and Pandis,
24 S. N.: Evaluation of the volatility basis-set approach for the simulation of organic aerosol formation
25 in the Mexico City metropolitan area, *Atmos. Chem. Phys.*, 10, 525–546, 25 doi:10.5194/acp-10-525-
26 2010, 2010.

27 Turpin, B. J. and Lim, H. J.: Species contributions to PM2.5 mass concentrations: revisiting common
28 assumptions for estimating organic mass, *Aerosol Sci. Tech.*, 35, 602–610,
29 doi:10.1080/02786820152051454, 2001.

30 Updyke, K. M., Nguyen, T. B., and Nizkorodov, S. A.: Formation of brown carbon via reactions of
31 ammonia with secondary organic aerosols from biogenic and anthropogenic precursors, *Atmos.*
32 *Environ.*, 63, 22–31, doi:10.1016/j.atmosenv.2012.09.012, 2012.

1 Valorso, R., Aumont, B., Camredon, M., Raventos-Duran, T., Mouchel-Vallon, C., Ng, N. L., Seinfeld, J.
2 H., Lee-Taylor, J., and Madronich, S.: Explicit modelling of SOA formation from a-pinene
3 photooxidation: sensitivity to vapour pressure estimation, *Atmos. Chem. Phys.*, 11, 6895–6910,
4 doi:10.5194/acp-11-6895-2011, 2011.

5 Vereecken, L. and Peeters, J.: Decomposition of substituted alkoxy radicals-part I: a generalized
6 structure–activity relationship for reaction barrier heights, *Phys. Chem. Chem. Phys.*, 11, 5 9062–
7 9074, doi:10.1039/b909712k, 2009.

8 Volkamer, R., Jimenez, J. L., San Martini, F., Dzepina, K., Zhang, Q., Salcedo, D., Molina, L. T.,
9 Worsnop, D. R., and Molina, M. J.: Secondary organic aerosol formation from anthropogenic air
10 pollution: rapid and higher than expected, *Geophys. Res. Lett.*, 33, L17811,
11 doi:10.1029/2006GL026899, 2006.

12 Volz, A. and Kley, D.: Evaluation of the Montsouris series of ozone measurements made in the
13 nineteenth century, *Nature*, 332, 240–242, doi:10.1038/332240a0, 1988.

14 Weininger, D.: SMILES, a chemical language and information-system .1. Introduction to methodology
15 and encoding rules, *J. Chem. Inf. Comp. Sci.*, 28, 31–36, doi:10.1021/ci00057a005, 1988.

16 Wolfe, G.M., Cantrell, C., Kim, S., Mauldin III, R. L., Karl, T., Turnipseed, A., Zheng, W., Flocke, F., Apel,
17 A. C., Hormbrook, R. S., Hall, S. R., Ullmann, K., Hemry, S. B., DiGanghil, J. P., Boyle, E. S., Kaser, L.,
18 Schnitzhofer, R., Hansel, A., Graus, M., Nakashima, Y., Kajii, Y., Guenther, A., and Keutsch, F. N.:
19 Missing peroxy radical sources within a summertime ponderosa pine forest, *Atmos. Chem. Phys.*, 14,
20 4715–4732, doi: 10.5194/acp-14-4715-2014, 2014.

21 Wood, E. C., Canagaratna, M. R., Herndon, S. C., Onasch, T. B., Kolb, C. E., Worsnop, D. R., Kroll, J. H.,
22 Knighton, W. B., Seila, R., Zavala, M., Molina, L. T., DeCarlo, P. F., Jimenez, J. L., Weinheimer, A. J.,
23 Knapp, D. J., Jobson, B. T., Stutz, J., Kuster, W. C., and Williams, E. J.: Investigation of the correlation
24 between odd oxygen and secondary organic aerosol in Mexico City and Houston, *Atmos. Chem. Phys.*,
25 10, 8947–8968, doi:10.5194/acp-10-8947-2010, 2010.

26 Yee, L. D., Craven, J. S., Loza, C. L., Schilling, K. A., Ng, N. L., Canagaratna, M. R., Ziemann, P. J.,
27 Flagan, R. C., and Seinfeld, J. H.: Secondary organic aerosol formation from low-NO_x photooxidation
28 of dodecane: evolution of multigeneration gas-phase chemistry and aerosol composition, *J. Phys.*
29 *Chem. A*, 116, 6211–6230, doi:10.1021/jp211531h, 2012.

30 Yee, L. D., Craven, J. S., Loza, C. L., Schilling, K. A., Ng, N. L., Canagaratna, M. R., Ziemann, P. J.,
31 Flagan, R. C., and Seinfeld, J. H.: Effect of chemical structure on secondary organic aerosol formation
32 from C12 alkanes, *Atmos. Chem. Phys.*, 13, 11121–11140, doi:10.5194/acp-13-11121-2013, 2013.

1 Yu, F.: A secondary organic aerosol formation model considering successive oxidation aging and
2 kinetic condensation of organic compounds: global scale implications, *Atmos. Chem. Phys.*, 11,
3 1083–1099, doi:10.5194/acp-11-1083-2011, 2011.

4 Zhang, Q., Jimenez, J. L., Canagaratna, M. R., Allan, J. D., Coe, H., Ulbrich, I., Alfarra, M. R., Takami, A.,
5 Middlebrook, A. M., Sun, Y. L., Dzepina, K., Dunlea, E., Docherty, K., DeCarlo, P. F., Salcedo, D.,
6 Onasch, T., Jayne, J. T., Miyoshi, T., Shimono, A., Hatakeyama, S., Takegawa, N., Kondo, Y., Schneider,
7 J., Drewnick, F., Borrmann, S., Weimer, S., Demerjian, K., Williams, P., Bower, K., Bahreini, R.,
8 Cottrell, L., Griffin, R. J., Rautiainen, J., Sun, J. Y., Zhang, Y. M., and Worsnop, D. R.: Ubiquity and
9 dominance of oxygenated species in organic aerosols in anthropogenically-influenced Northern
10 Hemisphere midlatitudes, *Geophys. Res. Lett.*, 34, L13801, doi:10.1029/2007GL029979, 2007.

11 Zhang, Q. J., Beekmann, M., Drewnick, F., Freutel, F., Schneider, J., Crippa, M., Prevot, A. S. H.,
12 Baltensperger, U., Poulain, L., Wiedensohler, A., Sciare, J., Gros, V., Borbon, A., Colomb, A., Michoud,
13 V., Doussin, J.-F., Denier van der Gon, H. A. C., Haeffelin, M., Dupont, J.-C., Siour, G., Petetin, H.,
14 Bessagnet, B., Pandis, S. N., Hodzic, A., Sanchez, O., Honoré, C., and Perrussel, O.: Formation of
15 organic aerosol in the Paris region during the MEGAPOLI summer campaign: evaluation of the
16 volatility-basis-set approach within the CHIMERE model, *Atmos. Chem. Phys.*, 13, 5767–5790,
17 doi:10.5194/acp-13-5767-2013, 2013.

1 Table 1. List of sensitivity simulations

Name	Conditions: urban (forest)
Base case	T = 291 K (288 K), dilution rate = 1 day ⁻¹ , seed aerosol = 2 $\mu\text{g m}^{-3}$ (1 $\mu\text{g m}^{-3}$), NAN vapor pressures, no dry deposition
T+10K	Outflow temperature = 301 K (298 K)
SLOWDIL	Dilution rate in outflow = 0.3 day ⁻¹ (0.46 day ⁻¹)
NODIL	Dilution rate in outflow = 0 day ⁻¹ (both scenarios)
SEED/2	Seed aerosol = 1 $\mu\text{g m}^{-3}$ (0.5 $\mu\text{g m}^{-3}$) during outflow
HV+	Increased photolysis : $j(\text{O}1\text{D}) \sim 100\% (\sim 35\%)$ higher
JRMY	Uses JRMY vapor pressures (urban case only), outflow T = 288K

2

1 Table 2. Carbon partitioning budget timeseries for the urban outflow simulation. Values are
 2 assessed at midnight on the days indicated. Losses are assessed relative to 4pm on day 1.
 3 Values < 100 are rounded to either two significant figures or two decimal places.

4

day	Particle phase carbon (mgC initial m ⁻³)				Gas phase carbon (mgC initial m ⁻³)				Net carbon loss (mgC initial m ⁻³)			
	C4- C9	C10- C15	C16- C21	C22- C30	C4- C9	C10- C15	C16- C21	C22- C30	C4- C9	C10- C15	C16- C21	C22- C30
1	0.88	0.61	1.9	1.8	171	7.3	2.1	0.29	4.0	0.12	0.04	0.01
2	1.9	1.6	2.7	2.0	146	5.5	1.0	0.14	27	1.0	0.25	0.01
3	2.4	2.5	3.1	2.0	122	3.5	0.48	0.07	52	2.1	0.47	0.02
4	3.3	3.2	3.2	2.1	92	1.4	0.17	0.03	80	3.4	0.67	0.03
5	4.0	3.5	3.1	2.1	65	0.44	0.07	0.02	107	4.2	0.81	0.04
6	4.3	3.4	3.1	2.1	47	0.19	0.05	0.01	125	4.5	0.90	0.05
7	4.5	3.3	3.0	2.1	36	0.11	0.04	0.01	136	4.6	0.96	0.06

1 Table 3. The top 20 contributors to modeled particle-phase production over the first 4 days¹ of the urban outflow simulation.

Rank	Formula	Unique SMILES ² name	Class ³	Notes/ MCM name ⁴	Precursor	p_{vap} (atm)	Contribution to production		
							Day 1	Day 4	4 days
1	C ₄ H ₄ O ₆	OOC1C(O)C(=O)OC1=O	MMAL	MALANHYOOH	aromatics	6.1E ⁻¹²	2.2%	23.0%	9.6%
2	C ₇ H ₈ O ₁₁ N ₂	CC12OOC(C1O[N](=O)=O)C(=C(O)C2(O)OO)[N](=O)=O	5f-PBN	MNNCATCOOH	toluene	1.3E ⁻¹³	0.9%	15.1%	5.9%
3	C ₇ H ₉ O ₉ N	CC12OOC(C1O)C(=C(O)C2(O)OO)[N](=O)=O	5f-PB	MNCATECOOH	toluene	2.6E ⁻¹³	0.2%	8.5%	3.1%
4	C ₅ H ₈ O ₆	CC(=O)C(O)C(=O)C(=O)=O	C<8	fragment ⁵	aromatics	2.5E ⁻¹¹	0.8%	0.2%	1.2%
5	C ₅ H ₇ O ₉ N	OOCC(=O)C(O)C(O)C(=O)OO[N](=O)=O	C<8,N	fragment	aromatics	2.7E ⁻¹²	0.5%	1.3%	1.2%
6	C ₈ H ₁₀ O ₁₁ N ₂	CC12OOC(C)(C1O[N](=O)=O)C(O)(OO)C(=C2[N](=O)=O)O	5f-PBN	MXNNCATOOH	m-xylene	1.0E ⁻¹³	0.4%	1.1%	1.1%
7	C ₅ H ₈ O ₆	CC(=O)C(=O)C(O)C(O)=O	C<8	fragment	aromatics	2.5E ⁻¹¹	0.8%	-	1.1%
8	C ₈ H ₁₀ O ₁₁ N ₂	CC1=C(O)C(O)(OO)C2(OOC1(C)C2O[N](=O)=O)[N](=O)=O	5f-PBN	OXNNCATOOH	o-xylene	9.5E ⁻¹⁴	0.2%	1.8%	1.1%
9	C ₅ H ₆ O ₆	CC1(OO)OCOC(=O)C1O	MMAL	MMALNHYOOH	aromatics	5.9E ⁻¹²	-	4.1%	1.0%
10	C ₈ H ₁₁ O ₈ N	CC1=CC(O)(OO)C2(OOC1(C)C2O)[N](=O)=O	4f-PB	TM124NOOH	1,2,4 TMB	2.9E ⁻¹¹	-	2.8%	0.9%
11	C ₇ H ₇ O ₁₂ N ₃	CC12OOC(C=C([N](=O)=O)C1(O)OO)(C2O[N](=O)=O)[N](=O)=O	5f-PBN	NDNCRESOOH	toluene	3.0E ⁻¹⁴	1.4%	0.9%	0.9%
12	C ₅ H ₅ O ₁₃ N ₃	OOCC(C(O[N](=O)=O)C(=O)OO[N](=O)=O)C(=O)OO[N](=O)=O	C<8,N	fragment	aromatics	2.2E ⁻¹¹	1.1%	-	0.9%
13	C ₅ H ₇ O ₈ N	CC(=O)C(O[N](=O)=O)C(=O)OO[C](=O)=O	C<8,N	fragment	aromatics	1.9E ⁻¹¹	1.5%	0.2%	0.8%
14	C ₈ H ₁₀ O ₁₁ N ₂	CC1=C(O)C(O)(OO)C2(C)OOC1(C2O[N](=O)=O)[N](=O)=O	5f-PBN	PXNNCATOOH	p-xylene	9.5E ⁻¹⁴	0.2%	1.1%	0.7%
15	C ₁₁ H ₂₁ O ₇ N	CCC(CCC(O)CC(=O)CCCOO)O[N](=O)=O	C>7,N	isomers ⁶	undecane	6.8E ⁻¹³	0.2%	0.9%	0.7%
16	C ₈ H ₁₀ O ₁₁ N ₂	CCC12OOC(C1O[N](=O)=O)C(=C(O)C2(O)OO)[N](=O)=O	5f-PBN	ENNCATCOOH	e-benzene	3.4E ⁻¹⁴	-	1.4%	0.6%
17	C ₈ H ₉ O ₁₂ N ₃	CC1=C([N](=O)=O)C2(OOC(C)(C2O[N](=O)=O)C1(O)OO)[N](=O)=O	5f-PBN	NDNMXYLOOH	m-xylene	1.9E ⁻¹⁴	-	0.5%	0.6%
18	C ₆ H ₉ O ₈ N	CC(=O)C(C)(OO)C(O[N](=O)=O)C(O)=O	C<8,N	fragment	aromatics	1.3E ⁻¹¹	0.8%	0.3%	0.5%
19	C ₇ H ₉ O ₈ N	CC12OOC(C1O)C(O)(OO)C(=C2)[N](=O)=O	4f-PB	TL4ONO2OOH	p-xylene	2.2E ⁻¹¹	-	1.6%	0.5%
20	C ₁₂ H ₂₃ O ₇ N	CCCC(CCC(O)CC(=O)CCCOO)O[N](=O)=O	C>7,N	isomers	dodecane	2.0E ⁻¹³	0.1%	0.6%	0.5%
Total ⁷ contribution to production							11.3%	65.4%	32.7%

2

3 Notes: ¹Days as used in this table are 24-hour periods beginning at 4pm. ²Unique SMILES notation is based on the original definition of Weininger (1988)

4 and referenced online at <http://cactus.nci.nih.gov/translate/>, February 2014. ³Class names are defined in the text. ⁴MCM names follow the notation of

5 Jenkin et al. (2003); Bloss et al. (2005b), as referenced online at <http://mcm.leeds.ac.uk/MCM>, February 2014. ⁵Fragmentation products shown here all have

1 several different aromatic precursors.⁶ Isomer lumping protocol is described by Valorso et al. (2011) and Aumont et al. (2008);⁷ The remainder consists of
2 species whose individual contributions are not in the top 20.

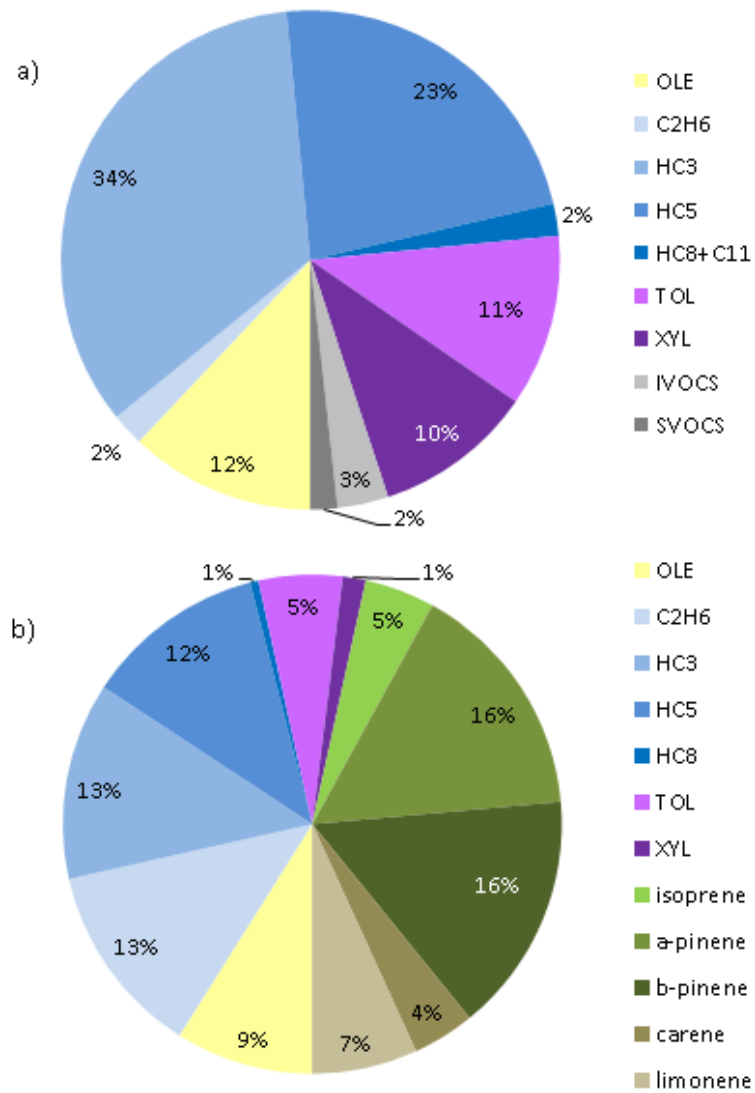
3

1 Table 4. The top 10 contributors to modeled particle mass at the end of the forest outflow simulation

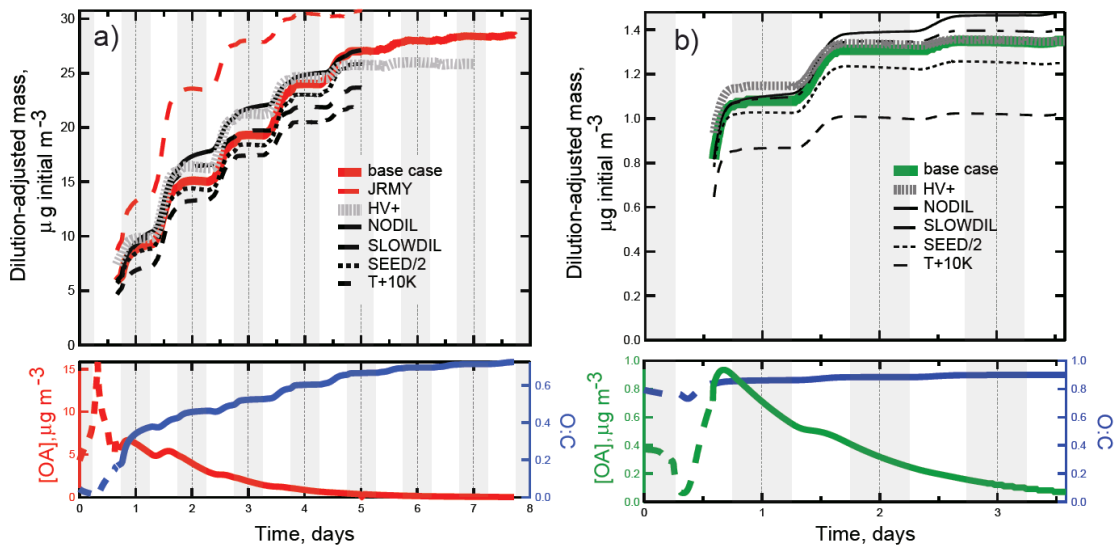
Rank	Formula	Unique SMILES ¹ name	Notes	Precursor	p_{vap} (atm)	Contribution to mass
1	C ₁₀ H ₁₈ O ₅	CC1(C)C(CCO)C(OO)C1C(=O)CO	6-member ring opened	β -pinene	7.7E ⁻¹²	2.4%
2	C ₅ H ₁₂ O ₆	CC(OO)C(O)C(CO)OO	Fragment	terpenes	2.7E ⁻¹²	2.0%
3	C ₁₀ H ₁₈ O ₆	CC(C)(C(CCO)OO)C(C=O)C(=O)CO	fully opened	β -pinene	1.8E ⁻¹³	1.5%
4	C ₁₀ H ₁₇ O ₇ N	C(C)(OO)C1CC(=O)CCC1(CO)O[N](=O)=O	4-member ring opened	β -pinene	5.8E ⁻¹²	1.3%
5	C ₅ H ₁₂ O ₆	CC(CO)(OO)C(O)COO	Fragment	limonene, isoprene	2.7E ⁻¹²	1.2%
6	C ₁₀ H ₁₇ O ₈ N	CC1(C)C2(O)CC(O[N](=O)=O)C(C)(OO)C1(C2)OO	2 rings, 4 substituents	α , β -pinene	8.3E ⁻¹⁴	1.2%
7	C ₁₀ H ₁₇ O ₈ N	CC(C)(OO)C(CCC(=O)CO)CC(=O)OO[N](=O)=O	fully opened	β -pinene, limonene	5.1E ⁻¹²	1.1%
8	C ₁₀ H ₁₇ O ₇ N	CC(C)(C(CCO)O[N](=O)=O)C(C=O)C(=O)CO	fully opened	β -pinene	3.4E ⁻¹²	1.1%
9	C ₁₀ H ₁₆ O ₉ N ₂	CC1(C)C2(O)CC1(CC(O[N](=O)=O)C2(C)O[N](=O)=O)OO	2 rings, 4 substituents	α -pinene	1.7E ⁻¹²	1.0%
10	C ₄ H ₄ O ₆	OOC1C(O)C(=O)OC1=O	MALANHYOOH ²	aromatics	6.1E ⁻¹²	0.9%
Total contribution to mass						13.6%

2

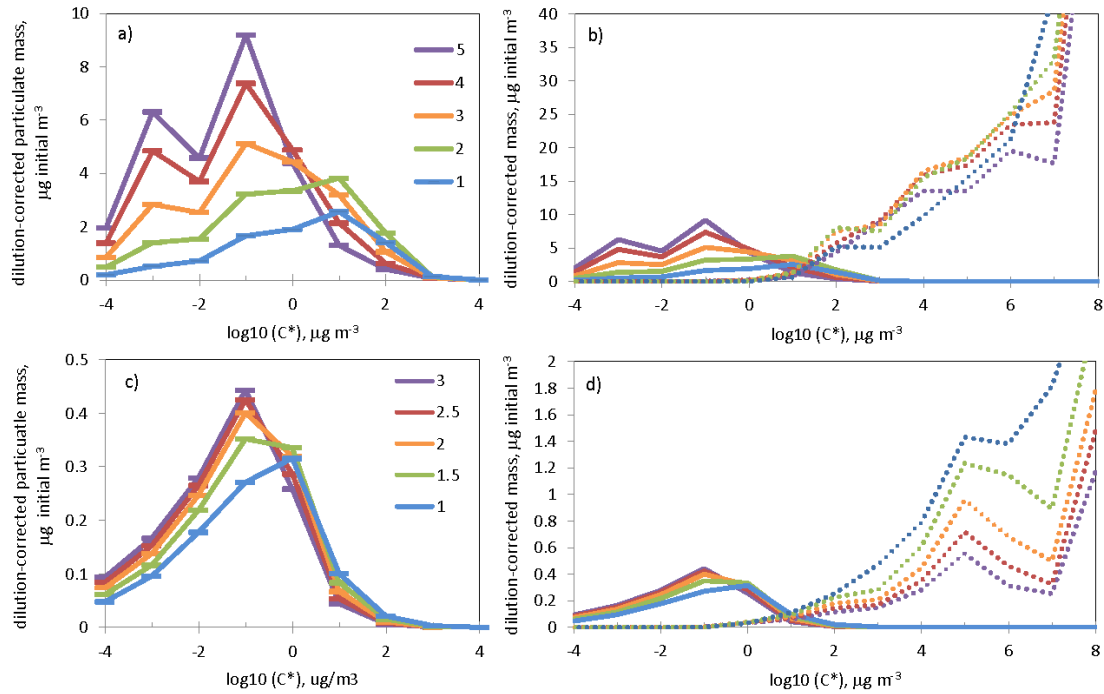
3 Notes: ¹Unique SMILES notation, see Table 2. ²MCM name, as in Table 2.



1
2 Figure 1. Precursor NMHC mass distributions for the outflow simulation runs. a) Urban case
3 emissions by mass. Total emissions are $2.6 \text{ g m}^{-2} \text{ day}^{-1}$. Species classes correspond loosely to those of
4 the RACM mechanism (Stockwell et al., 1997), and the volatility-based nomenclature of Donahue et
5 al. (2009). "OLE", olefins; "C2H6", ethane; "HC3", propane and similar species ; "HC5", n-pentane
6 and similar species; "HC8+C11", n-alkanes with 8 to 11 carbons, and cyclohexane; "TOL", toluene,
7 benzene, and ethyl benzene; "XYL", xylenes, trimethyl benzenes, and ethyl toluene; "IVOCS", n-
8 alkanes with 12 to 17 carbons; "SVOCS", n-alkanes with 18 to 30 carbons. Branched alkanes
9 constitute 16% and 66% of the mass in classes "HC3" and "HC5" respectively. b) Forest case
10 precursor inputs. Species classes are as in a). Inputs shown total $0.23 \text{ g m}^{-2} \text{ day}^{-1}$. Inputs of
11 oxygenated C1-4 species are omitted for clarity, and comprise an additional $0.7 \text{ g m}^{-2} \text{ day}^{-1}$ including
12 $0.2 \text{ g m}^{-2} \text{ day}^{-1}$ from methyl vinyl ketone and methyl butenol.

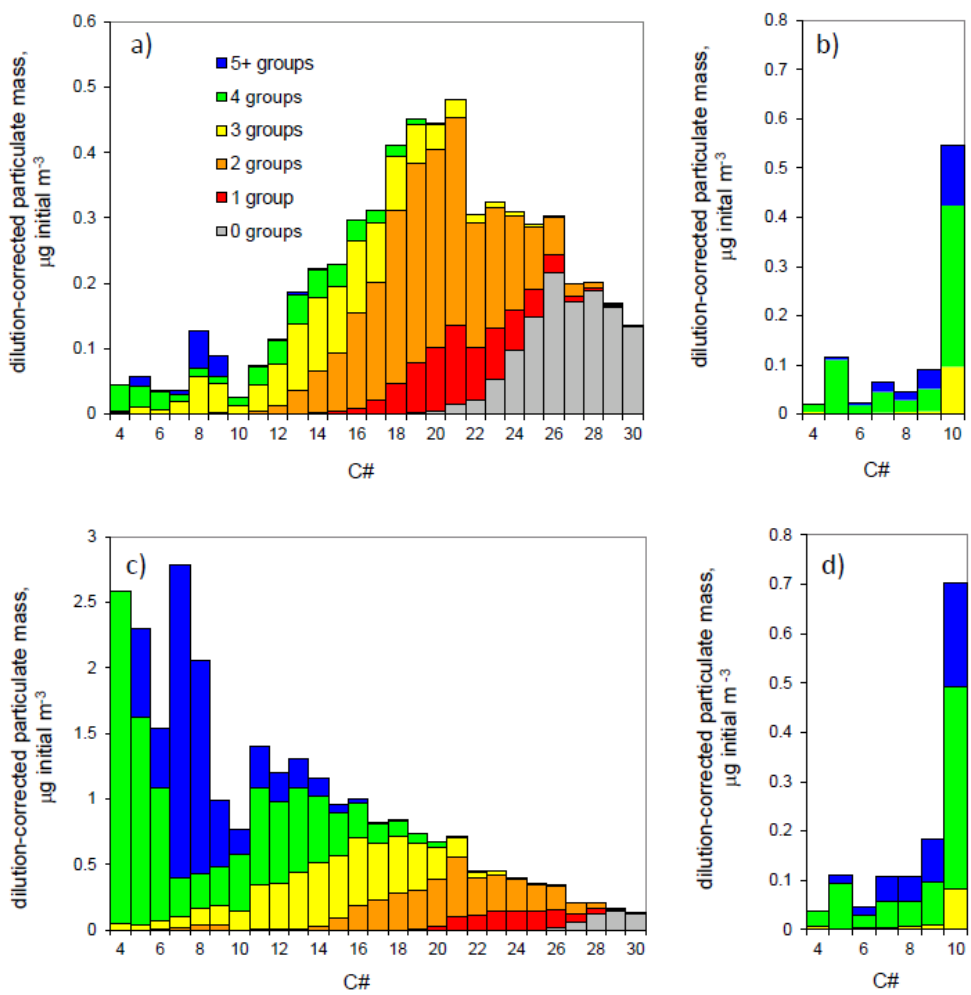


1
2 Figure 2. Simulated aerosol development for the a) urban and b) forest cases. Upper panels show
3 plume-integrated mass during the outflow phase, lower panels show concentrations and O:C ratios
4 for the model-generated aerosol fraction in the source regions and outflow phases. Grey shading
5 indicates approximate night-time periods.



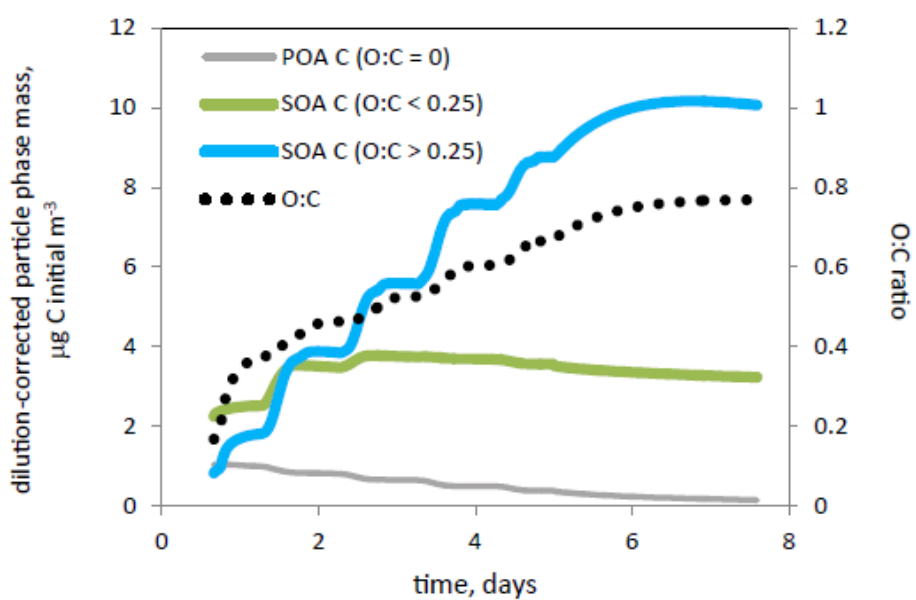
1

2 Figure 3. Time evolution of volatility distributions. a) and b) urban case; c) and d) forest case. Solid
 3 lines, particle phase; dotted lines, gas phases. Colors represent different times (see key): whole
 4 numbers are midnight values (e.g. “1” = midnight between days 1 and 2), and half-day numbers are
 5 noon values (e.g. “1.5” = noon on day 2). The volatility continuums have been binned in decadal
 6 increments for ease of comparison with so-called Volatility Basis Set (VBS) parameterizations.

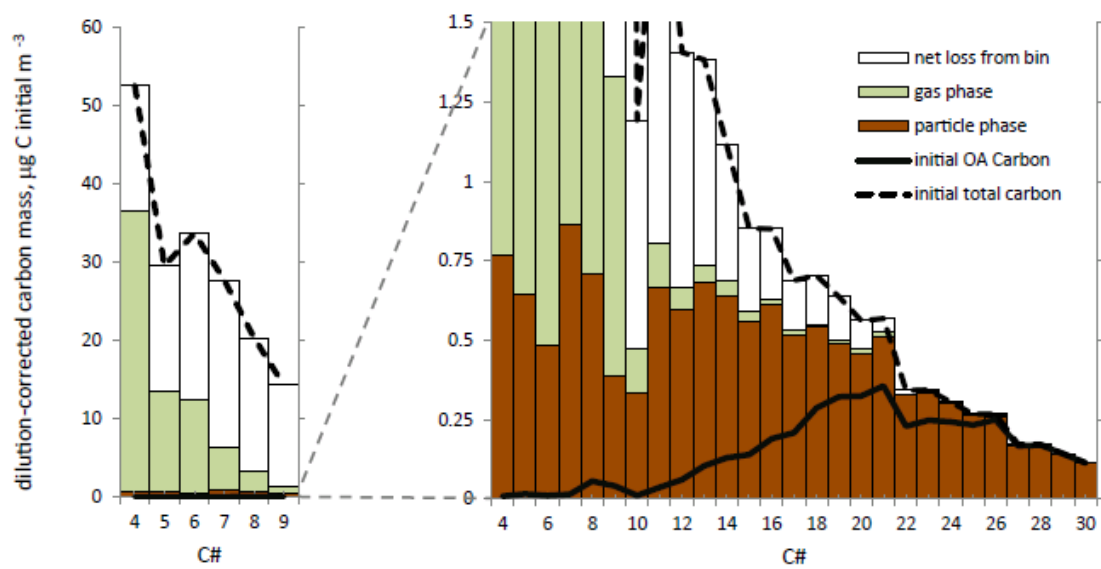


1

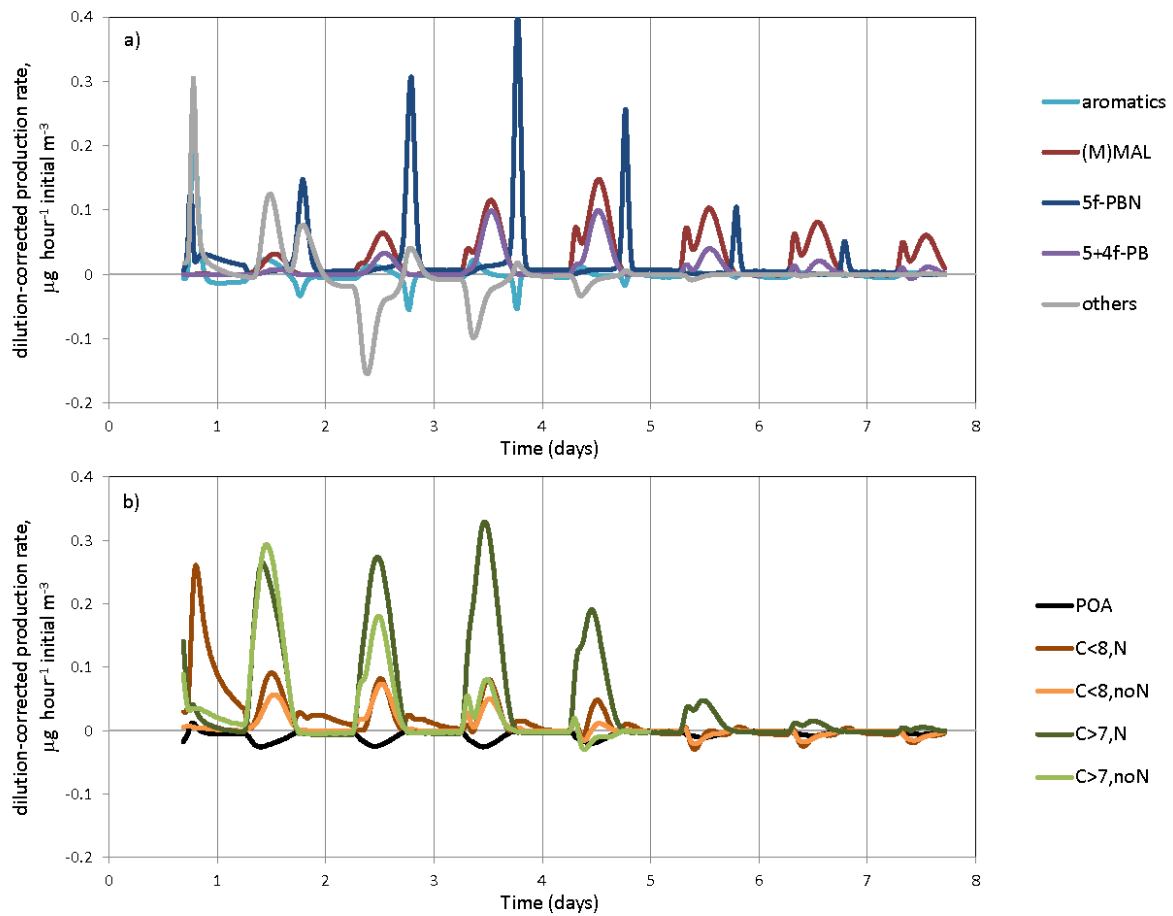
2 Figure 4. Particle mass composition binned by carbon number and number of functional groups per
3 constituent molecule. a) urban case at start of outflow phase; b) forest case at start of outflow
4 phase; c) urban case after 4 days; d) forest case after 3 days.



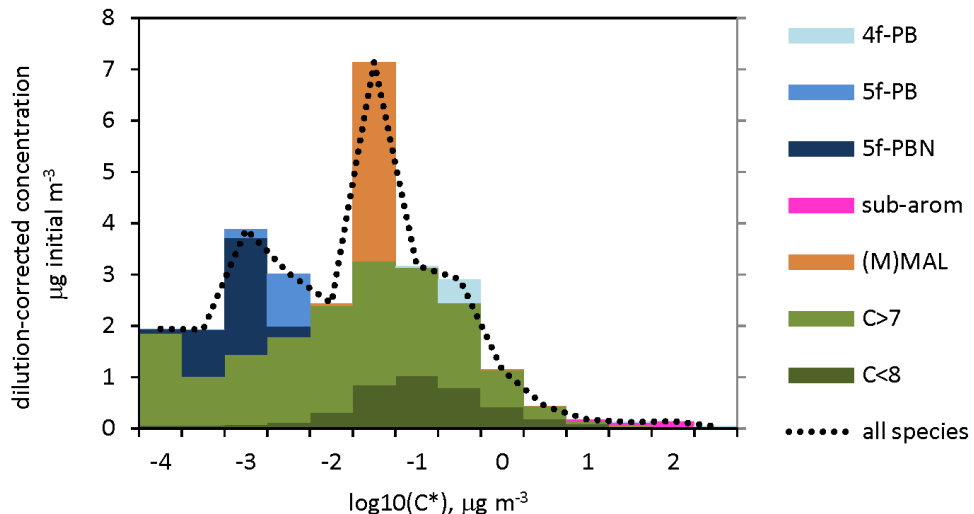
1
2 Figure 5. Evolution of the O:C ratio in the particle phase, for the urban case. Left axis and solid lines:
3 plume-integrated carbon mass of particle phase fractions, segregated by O:C ratio. Right axis and
4 black dotted line: O:C ratio of the entire particle phase.



1
 2 Figure 6. Carbon partitioning budget during the urban outflow simulation. Black lines show the gas
 3 (dashed line) and particle (solid line) phases at the start of outflow. Stacked bars show partitioning
 4 after 4 days: brown, particle phase; light green, persisting gas phase; white, net loss to
 5 fragmentation. Carbon numbers 4 to 9 are plotted twice, on different scales, to allow the details of
 6 the partitioning to be seen more clearly.



1
2 Figure 7. Hourly production rates of all species in the urban case particle phase, aggregated by broad
3 chemical characteristics. a) Cyclic products of aromatic precursors; b) all other species. Colors show
4 species groupings. See text for details.



1

2 Figure 8. Chemical composition of the particle phase at the end of the urban outflow simulation,
3 distributed by volatility. Colors show species groupings as discussed in the text: “C<8” and “C>7”,
4 linear/branched molecules separated by carbon number (no distinction for nitrate is made here);
5 “(M)MAL”, substituted maleic anhydrides; “sub-arom”, substituted rings that retain aromaticity; “5f-
6 PBN”, PBAs with 5 functional groups including nitrate; “5f-PB”, as 5f-PBN without nitrate; “4f-PB”,
7 PBAs with 4 functional groups. Dotted line shows total particle phase mass. The leftmost bin also
8 includes the mass from species with $\log_{10}(C^*) < -4$.

9